

Current bounds on the type-Z Z_3 three-Higgs-doublet model

Rafael Boto^{✉,*}, Jorge C. Romão^{✉,†} and João P. Silva^{✉,‡}

*Departamento de Física and CFTP, Instituto Superior Técnico Universidade de Lisboa,
Avenida Rovisco Pais 1, 1049-001 Lisboa, Portugal*

 (Received 27 July 2021; accepted 7 October 2021; published 10 November 2021)

Type-Z models, where charged leptons, up type quarks, and down type quarks each couple to a different scalar, are only possible when there are three or more Higgs doublets. We consider the type-Z three-Higgs-doublet model imposed by a softly broken Z_3 symmetry. We take into account all theoretical and experimental constraints, including perturbative unitarity and bounded from below conditions that we develop here. Since there can be cancellations between the two charged Higgs in $B \rightarrow X_s \gamma$ (and in $h \rightarrow \gamma \gamma$), the lower bounds obtained on the charged Higgs masses are alleviated. We find regions of parameter space where both charged scalars can be relatively light. We also discuss in detail the important physical differences between exact alignment and approximate alignment, and present some useful benchmark points.

DOI: [10.1103/PhysRevD.104.095006](https://doi.org/10.1103/PhysRevD.104.095006)

I. INTRODUCTION

After the observation in 2012 by ATLAS and CMS [1,2] of a new scalar particle closely resembling the Standard Model (SM) Higgs boson, the search for physics beyond the Standard Model (BSM) is now the main goal of the LHC experiments. Popular extensions where only Higgs doublets are added to the SM have been extensively studied and allow for both the agreement with the experimental results and the possibility of new features; for reviews see [3–5].

The simplest extension, the two-Higgs-doublet model (2HDM), can provide new sources of CP -violation necessary to fulfill the Sakharov criteria for baryogenesis [6]. However, the most general Higgs-fermion Yukawa couplings generically yield Higgs-mediated flavor-changing neutral “currents” (FCNCs) at tree level, in conflict with experimental observations. A common method to have FCNCs sufficiently suppressed is to impose symmetries on the Lagrangian: tree-level FCNC effects can be completely removed by establishing how the fermion and scalar fields have to transform under the chosen symmetry. In the 2HDM this can be achieved by imposing a Z_2 symmetry [7,8]. Reference [9] showed that in general N Higgs doublet models (NHDM) the Yukawa coupling matrices to fermions of a given electric charge remain proportional (thus

removing FCNCs) under the renormalization group running if and only if there is a basis for the Higgs doublets in which all the fermions of a given electric charge couple to only one Higgs doublet. The models are then classified based on these choices. The four (five) distinct types of Yukawa couplings in models with two (more than two) doublets that fit this requirement were introduced in [9] and denoted in [10] by Types I, II, X (also known as lepton-specific), Y (flipped), and Z, according to

$$\begin{aligned} \text{Type-I: } & \phi_u = \phi_d = \phi_e, \\ \text{Type-II: } & \phi_u \neq \phi_d = \phi_e, \\ \text{Type-X: } & \phi_u = \phi_d \neq \phi_e, \\ \text{Type-Y: } & \phi_u = \phi_e \neq \phi_d, \\ \text{Type-Z: } & \phi_u \neq \phi_d; \quad \phi_d \neq \phi_e, \quad \phi_e \neq \phi_u, \end{aligned} \quad (1)$$

where $\phi_{u,d,e}$ are the single scalar fields that couple exclusively to the up type quarks, down type quarks, and charged leptons, respectively. In this work, we set our attention on the type-Z that can only appear for NHDM with $N > 2$. It is interesting to see what differences there are in this new type of model, since it decouples completely the up quark, down quark and charged lepton sectors from one-another.

There have been implementations of type-Z in three-Higgs-doublet models (3HDM) using a $Z_2 \times Z_2$ symmetry [11,12] or Z_3 [13,14]. For this work, we choose to use a Z_3 symmetric potential. This symmetry is realizable through the following representation,

$$S_{Z_3} = \text{diag}(1, e^{i\frac{2\pi}{3}}, e^{-i\frac{2\pi}{3}}). \quad (2)$$

*rafael.boto@tecnico.ulisboa.pt
†jorge.romao@tecnico.ulisboa.pt
‡jpsilva@cftp.ist.utl.pt

Published by the American Physical Society under the terms of the [Creative Commons Attribution 4.0 International license](https://creativecommons.org/licenses/by/4.0/). Further distribution of this work must maintain attribution to the author(s) and the published article’s title, journal citation, and DOI. Funded by SCOAP³.

Recently, there has been an analysis of \mathbb{Z}_3 3HDM which takes the exact alignment limit and looks at specific values of the physical parameters [15]. It does not seem to consider the theoretical constraints coming from perturbative unitarity, discussed explicitly for the \mathbb{Z}_3 3HDM model in Ref. [16] and bounded from below (BFB) conditions, which guarantee that the potential does have a minimum and which we develop here. One important consideration that was studied in Ref. [15] was the impact of the experimental limits for the $\text{BR}(B \rightarrow X_s \gamma)$ on the masses of the charged Higgs scalars. This model has two charged Higgs scalars and they have shown that, for their constrained choice of parameters, the 2HDM limit on the charged Higgs mass [17] can be alleviated, which is an important result. This is shown in their Fig. 2, where the allowed regions in the charged Higgs masses plane are presented. However compatibility with the bounds coming from LHC searches for extra Higgs should also be checked. We do this here, using the newest version of the HiggsBounds-5.9.1 (HB5) code [18]. We show that recent LHC bounds on $h_{2,3} \rightarrow \tau^+ \tau^-$ decay in Ref. [19], already included in HiggsBounds-5.9.1, exclude all points in Ref. [15], for the same parameter choices. We then show that by scanning over a larger range of parameters (away from their exact alignment conditions, but still consistent with all experimental data) we can obtain viable points corresponding to smaller masses of the charged Higgs scalars.

In Sec. II we describe succinctly the scalar and Yukawa sectors of the \mathbb{Z}_3 3HDM model, discussed also in [13–15]. The theoretical and experimental constraints are described in Sec. III. In Sec. IV we describe the impact of current

LHC measurements on the 125 GeV scalar decays, both excluding and including the impact of HB5 bounds. In particular, we discuss the fact that the couplings of the 125 GeV Higgs boson (h_{125}) to two charged scalars may have different signs, thus allowing for canceling contributions to $h_{125} \rightarrow \gamma\gamma$. A similar effect is possible in $B \rightarrow X_s \gamma$, thus alleviating the lower bounds on charged scalar masses. This is discussed in Sec. V and Sec. VI, where we explore the regions of parameters allowed by the different constraints imposed, starting from the experimental limits on the $\text{BR}(B \rightarrow X_s \gamma)$ and progressively varying the ranges on our parameter scans. Our work highlights the importance of going beyond strict alignment, when procuring the full range of available parameter space and possible physical consequences within the \mathbb{Z}_3 3HDM. We present illustrative benchmark points in Sec. VIII and discuss our conclusions in Sec. IX, leaving the Appendixes for the full expression of some couplings required in our calculations and a detailed study of $\sigma(pp \rightarrow h_2) \times \text{BR}(h_2 \rightarrow \tau\tau)$.

II. THE \mathbb{Z}_3 3HDM MODEL

A. Scalar sector

Taking the potential defined by [13], the terms invariant under the chosen transformation, $\phi_i \rightarrow \phi'_i = (S_{\mathbb{Z}_3})_{ij} \phi_j$, are given by

$$V_{\mathbb{Z}_3} = V_{\text{quadratic}} + V_{\text{quartic}}, \quad (3)$$

with the quartic part

$$\begin{aligned} V_{\text{quartic}} = & \lambda_1(\phi_1^\dagger \phi_1)^2 + \lambda_2(\phi_2^\dagger \phi_2)^2 + \lambda_3(\phi_3^\dagger \phi_3)^2 + \lambda_4(\phi_1^\dagger \phi_1)(\phi_2^\dagger \phi_2) + \lambda_5(\phi_1^\dagger \phi_1)(\phi_3^\dagger \phi_3) \\ & + \lambda_6(\phi_2^\dagger \phi_2)(\phi_3^\dagger \phi_3) + \lambda_7(\phi_1^\dagger \phi_2)(\phi_2^\dagger \phi_1) + \lambda_8(\phi_1^\dagger \phi_3)(\phi_3^\dagger \phi_1) + \lambda_9(\phi_2^\dagger \phi_3)(\phi_3^\dagger \phi_2) \\ & + [\lambda_{10}(\phi_1^\dagger \phi_2)(\phi_1^\dagger \phi_3) + \lambda_{11}(\phi_1^\dagger \phi_2)(\phi_3^\dagger \phi_2) + \lambda_{12}(\phi_1^\dagger \phi_3)(\phi_2^\dagger \phi_3) + \text{H.c.}], \end{aligned} \quad (4)$$

The quadratic part is

$$\begin{aligned} V_{\text{quadratic}} = & m_{11}^2 \phi_1^\dagger \phi_1 + m_{22}^2 \phi_2^\dagger \phi_2 + m_{33}^2 \phi_3^\dagger \phi_3 \\ & + [m_{12}^2 (\phi_1^\dagger \phi_2) + m_{13}^2 (\phi_1^\dagger \phi_3) \\ & + m_{23}^2 (\phi_2^\dagger \phi_3) + \text{H.c.}], \end{aligned} \quad (5)$$

where we also include terms, m_{12}^2 , m_{13}^2 , and m_{23}^2 , that break the symmetry softly.

After spontaneous symmetry breaking (SSB), the three doublets can be parametrized in terms of its component fields as¹:

¹Notice that we use x_i in place of Ref. [13]'s h_i , because for us h_i are the physical neutral scalar mass eigenstates.

$$\phi_i = \begin{pmatrix} w_k^\dagger \\ (v_i + x_i + iz_i)/\sqrt{2} \end{pmatrix}, \quad (i = 1, 2, 3) \quad (6)$$

where $v_i/\sqrt{2}$ corresponds to the vacuum expectation value (vev) for the neutral component of ϕ_i . It is assumed that the scalar sector of the model explicitly and spontaneously conserves CP .²

²Strictly speaking, it is not advisable to assume a real scalar sector while allowing the Yukawa couplings to carry the phase necessary for the CKM matrix. This is also a problem with the so-called real 2HDM [20]. One can take the view that the complex terms and their counterterms in the scalar sector exist, with the former set to zero.

That is, all the parameters in the scalar potential are real and the vevs v_1, v_2, v_3 , are also real. With this assumption, the scalar potential of Eq. (3) contains eighteen parameters. The vevs can be parametrized as follows:

$$v_1 = v \cos \beta_1 \cos \beta_2, \quad v_2 = v \sin \beta_1 \cos \beta_2, \quad v_3 = v \sin \beta_2, \quad (7)$$

leading to the Higgs basis [21–23] to be obtained by the following rotation,

$$\begin{pmatrix} H_0 \\ R_1 \\ R_2 \end{pmatrix} = \mathcal{O}_\beta \begin{pmatrix} x_1 \\ x_2 \\ x_3 \end{pmatrix} = \begin{pmatrix} \cos \beta_2 \cos \beta_1 & \cos \beta_2 \sin \beta_1 & \sin \beta_2 \\ -\sin \beta_1 & \cos \beta_1 & 0 \\ -\cos \beta_1 \sin \beta_2 & -\sin \beta_1 \sin \beta_2 & \cos \beta_2 \end{pmatrix} \begin{pmatrix} x_1 \\ x_2 \\ x_3 \end{pmatrix}. \quad (8)$$

The scalar kinetic Lagrangian is written as

$$\mathcal{L}_{\text{kin}} = \sum_{k=1}^{n=3} |D_\mu \phi_k|^2, \quad (9)$$

and contains the terms relevant to the propagators and trilinear couplings of the scalars and gauge bosons.

We can now define orthogonal matrices which diagonalize the squared-mass matrices present in the CP -even scalar, CP -odd scalar, and charged scalar sectors. These are the transformations that take us to the physical basis, with states possessing well-defined masses. Following Ref. [13,14], the twelve quartic couplings can be exchanged for seven physical masses (three CP -even scalars, two CP -odd scalars and two pairs of charged scalars) and five mixing angles. The mass terms in the neutral scalar sector can be extracted through the following rotation,

$$\begin{pmatrix} h_1 \\ h_2 \\ h_3 \end{pmatrix} = \mathcal{O}_\alpha \begin{pmatrix} x_1 \\ x_2 \\ x_3 \end{pmatrix}, \quad (10)$$

where we take $h_1 \equiv h_{125}$ to be the 125 GeV Higgs particle found at LHC. The form chosen for \mathcal{O}_α is

$$\mathbf{R} \equiv \mathcal{O}_\alpha = \mathcal{R}_3 \cdot \mathcal{R}_2 \cdot \mathcal{R}_1, \quad (11)$$

where

$$\mathcal{R}_1 = \begin{pmatrix} c_{\alpha_1} & s_{\alpha_1} & 0 \\ -s_{\alpha_1} & c_{\alpha_1} & 0 \\ 0 & 0 & 1 \end{pmatrix}, \quad \mathcal{R}_2 = \begin{pmatrix} c_{\alpha_2} & 0 & s_{\alpha_2} \\ 0 & 1 & 0 \\ -s_{\alpha_2} & 0 & c_{\alpha_2} \end{pmatrix},$$

$$\mathcal{R}_3 = \begin{pmatrix} 1 & 0 & 0 \\ 0 & c_{\alpha_3} & s_{\alpha_3} \\ 0 & -s_{\alpha_3} & c_{\alpha_3} \end{pmatrix}. \quad (12)$$

For the CP -odd scalar sector, the physical basis is chosen as $(G^0 \ A_1 \ A_2)^T$ and the transformation to be

$$\begin{pmatrix} G^0 \\ A_1 \\ A_2 \end{pmatrix} = \mathcal{O}_{\gamma_1} \mathcal{O}_\beta \begin{pmatrix} z_1 \\ z_2 \\ z_3 \end{pmatrix}, \quad (13)$$

where

$$\mathcal{O}_{\gamma_1} = \begin{pmatrix} 1 & 0 & 0 \\ 0 & c_{\gamma_1} & -s_{\gamma_1} \\ 0 & s_{\gamma_1} & c_{\gamma_1} \end{pmatrix}. \quad (14)$$

is defined in order to diagonalize the 2×2 submatrix that remains nondiagonal in the Higgs basis. For later use, we define the matrix \mathbf{P} as the combination

$$\mathbf{P} \equiv \mathcal{O}_{\gamma_1} \mathcal{O}_\beta. \quad (15)$$

For the charged scalar sector, the physical basis is $(G^+ \ H_1^+ \ H_2^+)^T$ and the transformation is

$$\begin{pmatrix} G^+ \\ H_1^+ \\ H_2^+ \end{pmatrix} = \mathcal{O}_{\gamma_2} \mathcal{O}_\beta \begin{pmatrix} w_1^\dagger \\ w_2^\dagger \\ w_3^\dagger \end{pmatrix}, \quad (16)$$

where

$$\mathcal{O}_{\gamma_2} = \begin{pmatrix} 1 & 0 & 0 \\ 0 & c_{\gamma_2} & -s_{\gamma_2} \\ 0 & s_{\gamma_2} & c_{\gamma_2} \end{pmatrix}. \quad (17)$$

We write the masses of H_1^+ and H_2^+ as $m_{H_1^\pm}$ and $m_{H_2^\pm}$, respectively. The matrix \mathbf{Q} is then defined as the combination

$$\mathbf{Q} \equiv \mathcal{O}_{\gamma_2} \mathcal{O}_\beta. \quad (18)$$

Considering that the states in the physical basis have well-defined masses, we can obtain relations between the set

$$\{v_1, v_2, v_3, m_{h_1}, m_{h_2}, m_{h_3}, m_{A_1}, m_{A_2}, m_{H_1^\pm}, m_{H_2^\pm}, \alpha_1, \alpha_2, \alpha_3, \gamma_1, \gamma_2\}, \quad (19)$$

$$v_1 = v \cos \beta_1 \cos \beta_2, \quad v_2 = v \sin \beta_1 \cos \beta_2, \quad v_3 = v \sin \beta_2, \quad (20)$$

and the parameters of the potential in Eq. (3), as shown in Ref. [13,14]. We performed an extensive scan of the parameter space in Eq. (19). Our fixed inputs are $v = 246$ GeV and $m_{h_1} = 125$ GeV. We then took random values in the ranges:

$$\begin{aligned} \alpha_1, \alpha_2, \alpha_3, \gamma_1, \gamma_2 &\in \left[-\frac{\pi}{2}, \frac{\pi}{2}\right]; & \tan \beta_1, \tan \beta_2 &\in [0, 10]; \\ m_{h_2}, m_{h_3} &\in [125, 1000] \text{ GeV}; & m_{A_1}, m_{A_2}, m_{H_1^\pm}, m_{H_2^\pm} &\in [100, 1000] \text{ GeV}. \end{aligned} \quad (21)$$

These parameter ranges will be used in all scans and figures presented below, except where noted otherwise. The lower limits chosen for the masses satisfy the constraints listed in Ref. [24].³

B. Higgs-Fermion Yukawa interactions

One can now impose the type-Z model on the Yukawa Lagrangian, by establishing how the fields behave under the \mathbb{Z}_3 transformation. For this, there are multiple possibilities that differ on which of the scalars gives mass to each type of fermion. We follow the choice made by Das and Saha [13]. The scalar doublets ϕ_1 and ϕ_2 transform nontrivially as:

$$\phi_1 \rightarrow \omega \phi_1, \quad \phi_2 \rightarrow \omega^2 \phi_2, \quad (22)$$

where $\omega = e^{2\pi i/3}$. For the fermionic fields, we consider that under \mathbb{Z}_3

$$d_R \rightarrow \omega d_R, \quad l_R \rightarrow \omega^2 l_R, \quad (23)$$

while the rest of the fields remain unaffected. It follows that the Yukawa coupling matrices are now restricted: ϕ_1 only has interaction terms with the charged leptons, giving them mass; ϕ_3 and ϕ_2 are responsible for masses of the up and down type quarks, respectively.

When taking into account the restrictions imposed by the symmetry, the Yukawa couplings to fermions can be written in a compact form. For the couplings of neutral Higgs to fermions,

$$\mathcal{L}_Y \ni -\frac{m_f}{v} \bar{f} (a_j^f + i b_j^f \gamma_5) f h_j, \quad (24)$$

where we group the physical Higgs fields in a vector, as $h_j \equiv (h_1, h_2, h_3, A_1, A_2)_j$. The coefficients are given in Eq. (25),

$$\begin{aligned} a_j^f &\rightarrow \frac{\mathbf{R}_{j,1}}{\hat{v}_1}, \quad j = 1, 2, 3 \quad \text{for all leptons,} \\ b_j^f &\rightarrow \frac{\mathbf{P}_{j-2,1}}{\hat{v}_1}, \quad j = 4, 5 \quad \text{for all leptons,} \\ a_j^f &\rightarrow \frac{\mathbf{R}_{j,3}}{\hat{v}_3}, \quad j = 1, 2, 3 \quad \text{for all up quarks,} \\ b_j^f &\rightarrow -\frac{\mathbf{P}_{j-2,3}}{\hat{v}_3}, \quad j = 4, 5 \quad \text{for all up quarks,} \\ a_j^f &\rightarrow \frac{\mathbf{R}_{j,2}}{\hat{v}_2}, \quad j = 1, 2, 3 \quad \text{for all down quarks,} \\ b_j^f &\rightarrow \frac{\mathbf{P}_{j-2,2}}{\hat{v}_2}, \quad j = 4, 5 \quad \text{for all down quarks,} \end{aligned} \quad (25)$$

where we introduce $\hat{v}_i = v_i/v$, with the vevs in Eq. (7). Note how the coupling of each type of fermion depends on entries of the diagonalization matrices in Eqs. (11) and (15).

The couplings of the charged Higgs, H_1^\pm and H_2^\pm , to fermions can be expressed as

$$\begin{aligned} \mathcal{L}_Y \ni &\frac{\sqrt{2}}{v} \bar{\psi}_{d_i} [m_{\psi_{d_i}} V_{ji}^* \eta_k^L P_L + m_{\psi_{u_j}} V_{ji}^* \eta_k^R P_R] \psi_{u_j} H_k^- \\ &+ \frac{\sqrt{2}}{v} \bar{\psi}_{u_i} [m_{\psi_{d_j}} V_{ij} \eta_k^L P_R + m_{\psi_{u_i}} V_{ij} \eta_k^R P_L] \psi_{d_j} H_k^+, \end{aligned} \quad (26)$$

where (ψ_{u_i}, ψ_{d_i}) is (u_i, d_i) for quarks or (ν_i, l_i) for leptons. For quarks, V is the CKM matrix, while for leptons, $V_{ij} = \delta_{ij}$ since we are considering massless neutrinos. The couplings are

$$\begin{aligned} \eta_k^{lL} &= -\frac{\mathbf{Q}_{k+1,1}}{\hat{v}_1}, \quad \eta_k^{lR} = 0, \quad \eta_k^{qL} = -\frac{\mathbf{Q}_{k+1,2}}{\hat{v}_2}, \\ \eta_k^{qR} &= \frac{\mathbf{Q}_{k+1,3}}{\hat{v}_3}, \quad k = 1, 2, \end{aligned} \quad (27)$$

for leptons and quarks, respectively.

³Reference [24] has the same \mathbb{Z}_3 3HDM scalar sector, but it does not couple to fermions as a type-Z model because the aim there is to have two Inert scalar doublets and only one active one.

III. CONSTRAINTS ON THE PARAMETER SPACE

In this section we study the constraints that must be applied to the model parameters in order to ensure consistency.

A. Theoretical constraints 1

We impose perturbativity unitarity, sufficient bounded from below conditions, and the oblique parameters S , T , and U .

1. BFB conditions on the 3HDM

As basic requirements for any physical theory, the Higgs potential must satisfy conditions that ensure it possesses a stable minimum, around which one can perform perturbative calculations. That is, it must be bounded from below, meaning that there is no direction in field space along which the value of the potential tends to minus infinity. This need of a nontrivial minimum is then translated into conditions on the parameters of the potential.

Focusing on the study of the 3HDM constrained by a Z_3 symmetry, the quartic terms in Eq. (4) can be written as

$$V_{\text{quartic}} = V_0 + V_1, \quad (28)$$

where V_0 has the terms in $\lambda_{1 \rightarrow 9}$ and V_1 the terms $\lambda_{10 \rightarrow 12}$. If the potential were just V_0 in Eq. (28), then the BFB necessary and sufficient conditions would be simply those given by Klimenko in Ref. [25]. The problem, not yet solved for the 3HDM with a Z_3 symmetry is the V_1 part. We will introduce sufficient conditions for BFB by bounding the potential by a lower potential. To do that we follow [25,26], checking for neutral minima. Neutral directions in the Higgs space correspond to situations when all ϕ_i are proportional to each other.⁴ Along these directions, we can then define

$$\phi_1 \rightarrow \sqrt{x}e^{i\theta_1}, \quad \phi_2 \rightarrow \sqrt{y}e^{i\theta_2}, \quad \phi_3 \rightarrow \sqrt{z}e^{i\theta_3}. \quad (29)$$

It then follows that for V_0 ,

$$\begin{aligned} V_0 &= \lambda_1 x^2 + \lambda_2 y^2 + \lambda_3 z^2 + \lambda_4 xy + \lambda_5 xz + \lambda_6 yz \\ &\quad + \lambda_7 xy + \lambda_8 xz + \lambda_9 yz \\ &= \lambda_1 x^2 + \lambda_2 y^2 + \lambda_3 z^2 + (\lambda_4 + \lambda_7)xy \\ &\quad + (\lambda_5 + \lambda_8)xz + (\lambda_6 + \lambda_9)yz, \end{aligned} \quad (30)$$

⁴Other directions, along which the strict proportionality of all three doublets does not hold, are called *charge-breaking* (CB) directions. In recent works [27,28], it has been proven that these directions can lead to pathological situations for other symmetries in the 3HDM. It is then required to consider these directions when doing a complete work of looking for necessary and sufficient BFB conditions. Our contribution to the analysis of the Z_3 symmetry is to specify sufficient conditions along the neutral direction.

and for V_1 ,

$$\begin{aligned} V_1 &= 2\lambda_{10}x\sqrt{y}\sqrt{z}\cos\delta_1 + 2\lambda_{11}y\sqrt{x}\sqrt{z}\cos\delta_2 \\ &\quad + 2\lambda_{12}z\sqrt{x}\sqrt{y}\cos\delta_3, \end{aligned} \quad (31)$$

where δ_i are some combination of the phases θ_i . Considering that $x, y, z > 0$ by definition, we can start our strategy of bounding the potential by a lower one with

$$V_1 \geq V'_1 = -2|\lambda_{10}|x\sqrt{y}\sqrt{z} - 2|\lambda_{11}|y\sqrt{x}\sqrt{z} - 2|\lambda_{12}|z\sqrt{x}\sqrt{y}. \quad (32)$$

Notice that for non-negative x, y, z one has

$$-\sqrt{x}\sqrt{z} > -x - y, \quad -\sqrt{x}\sqrt{z} > -x - z, \quad -\sqrt{y}\sqrt{z} > -y - z. \quad (33)$$

Therefore,

$$\begin{aligned} V_1 \geq V'_1 > V''_1 &= -2|\lambda_{10}|(xy + xz) - 2|\lambda_{11}|(xy + yz) \\ &\quad - 2|\lambda_{12}|(xz + yz), \end{aligned} \quad (34)$$

and combining Eq. (34) with Eq. (30), it follows that

$$V_0 + V_1 > V_{\text{BFB}}, \quad (35)$$

where

$$V_{\text{BFB}} = \lambda_1 x^2 + \lambda_2 y^2 + \lambda_3 z^2 + 2\alpha xy + 2\beta xz + 2\gamma yz, \quad (36)$$

with the definitions,

$$\begin{aligned} \alpha &= \frac{1}{2}(\lambda_4 + \lambda_7 - 2|\lambda_{10}| - 2|\lambda_{11}|), \\ \beta &= \frac{1}{2}(\lambda_5 + \lambda_8 - 2|\lambda_{10}| - 2|\lambda_{12}|), \\ \gamma &= \frac{1}{2}(\lambda_6 + \lambda_9 - 2|\lambda_{11}| - 2|\lambda_{12}|). \end{aligned} \quad (37)$$

Now, for the potential V_{BFB} the necessary and sufficient conditions are obtained from Ref. [25]:

- (i) $\lambda_1 > 0, \lambda_2 > 0, \lambda_3 > 0,$
- (ii) $\left\{ \beta > -\sqrt{\lambda_1 \lambda_3}; \gamma > -\sqrt{\lambda_2 \lambda_3}; \alpha > -\sqrt{\lambda_1 \lambda_2}; \right.$
 $\left. \beta \geq -\gamma\sqrt{\lambda_1/\lambda_2} \right\} \cup \left\{ \sqrt{\lambda_2 \lambda_3} > \gamma > -\sqrt{\lambda_2 \lambda_3}; \right.$
 $\left. -\gamma\sqrt{\lambda_1/\lambda_2} \geq \beta > -\sqrt{\lambda_1 \lambda_3}; \lambda_3 \alpha > \beta\gamma - \sqrt{\Delta_\alpha \Delta_\gamma} \right\},$

where

$$\Delta_\alpha = \beta^2 - \lambda_1 \lambda_3, \quad \Delta_\gamma = \gamma^2 - \lambda_2 \lambda_3. \quad (39)$$

As $V_0 + V_1 > V_{\text{BFB}}$, these conditions are sufficient conditions for the original potential. They are not necessary, and therefore might be throwing away part of the parameter space. However, it still gives us a very good sense of the possibilities within the type-Z 3HDM.

2. Unitarity

In order to determine the tree-level unitarity constraints, we use the algorithm presented in [16]. As described there, we have to impose that the eigenvalues of the scattering S-matrix of two scalars into two scalars have an upper bound (the unitarity limit). As these arise exclusively from the quartic part of the potential, the eigenvalues obtained for a \mathbb{Z}_3 symmetric potential in Section 4.4 of [16] can also be used for the potential with quadratic soft-breaking terms, Eq. (3). The conversion between the notation of the algorithm and the potential chosen, Eq. (4), is as follows:

$$r_1 \rightarrow \lambda_1, \quad r_2 \rightarrow \lambda_2, \quad r_3 \rightarrow \lambda_3, \quad (40)$$

$$r_4 \rightarrow \lambda_4/2, \quad r_5 \rightarrow \lambda_5/2, \quad r_6 \rightarrow \lambda_6/2, \quad (41)$$

$$r_7 \rightarrow \lambda_7/2, \quad r_8 \rightarrow \lambda_8/2, \quad r_9 \rightarrow \lambda_9/2, \quad (42)$$

$$c_4 \rightarrow \lambda_{10}/2, \quad c_{12} \rightarrow \lambda_{11}/2, \quad c_{11} \rightarrow \lambda_{12}/2. \quad (43)$$

Denoting by Λ_i the eigenvalues of the relevant scattering matrices, we have 21 Λ 's to calculate for each set of physical parameters randomly generated, and the condition to impose is that

$$|\Lambda_i| \leq 8\pi, \quad i = 1, \dots, 21. \quad (44)$$

3. Oblique parameters STU

In order to discuss the effect of the S , T , U parameters, we use the results in [29]. To apply the relevant expressions, we write the matrices U and V used in [29] with the notation choices that we made when obtaining the mass eigenstates in Sec. II A. We start with the 3×6 matrix V defined as

$$\begin{pmatrix} x_1 + iz_1 \\ x_2 + iz_2 \\ x_3 + iz_3 \end{pmatrix} = V \begin{pmatrix} G^0 \\ h_1 \\ h_2 \\ h_3 \\ A_1 \\ A_2 \end{pmatrix}, \quad (45)$$

and find, by comparison with Eqs. (10) and (13), that V is

$$V = \begin{pmatrix} i\mathbf{P}_{11}^T & \mathbf{R}_{11}^T & \mathbf{R}_{12}^T & \mathbf{R}_{13}^T & i\mathbf{P}_{12}^T & i\mathbf{P}_{13}^T \\ i\mathbf{P}_{21}^T & \mathbf{R}_{21}^T & \mathbf{R}_{22}^T & \mathbf{R}_{23}^T & i\mathbf{P}_{22}^T & i\mathbf{P}_{23}^T \\ i\mathbf{P}_{31}^T & \mathbf{R}_{31}^T & \mathbf{R}_{32}^T & \mathbf{R}_{33}^T & i\mathbf{P}_{32}^T & i\mathbf{P}_{33}^T \end{pmatrix}. \quad (46)$$

The 3×3 matrix U defined as

$$\begin{pmatrix} w_1^\dagger \\ w_2^\dagger \\ w_3^\dagger \end{pmatrix} = U \begin{pmatrix} G^\dagger \\ H_1^\dagger \\ H_2^\dagger \end{pmatrix}, \quad (47)$$

gives us the correspondence $U = \mathbf{Q}^T$ from Eq. (16).

Having applied the expressions for S , T , U , the constraints implemented on S and T follow Ref. [30], at 95% confidence level. For U , we fix the allowed interval to be

$$U = 0.03 \pm 0.10. \quad (48)$$

B. Theoretical constraints 2

As we want to explore the range of low $\tan \beta_1$ and $\tan \beta_2$ we should avoid that the Yukawa couplings become non-perturbative. We have, in our model

$$Y_t = \frac{m_t \sqrt{2}}{v} \frac{\sqrt{1 + \tan \beta_2^2}}{\tan \beta_2}, \quad (49)$$

$$Y_\tau = \frac{m_\tau \sqrt{2}}{v} \sqrt{1 + \tan \beta_1^2} \sqrt{1 + \tan \beta_2^2}, \quad (50)$$

$$Y_b = \frac{m_b \sqrt{2}}{v} \frac{\sqrt{1 + \tan \beta_1^2} \sqrt{1 + \tan \beta_2^2}}{\tan \beta_1}. \quad (51)$$

We require

$$\frac{Y^2}{4\pi} < 1 \Rightarrow Y < \sqrt{4\pi} \quad (52)$$

C. $\Delta M_{b,s}$ Constraints

We see from Ref. [15] that the constraints coming from $\Delta M_{b,s}$ tend to exclude very low values on $\tan \beta$. Thus, we take

$$\log_{10}(\tan \beta_{1,2}) > -0.5 \Rightarrow \tan \beta_{1,2} > 10^{-0.5} = 0.31623. \quad (53)$$

D. LHC constraints

For comparison with experiment, we consider only the contributions of the lowest nonvanishing order in perturbation theory. The decays that require one-loop calculations

are those of neutral scalars into two photons ($h_j \rightarrow \gamma\gamma$), one Z and one photon ($h_j \rightarrow Z\gamma$), and two gluons ($h_j \rightarrow gg$). The final formulas for the first two widths are given in Ref. [31], only having to adapt the particles and their couplings to our case. The formula for the width $h_j \rightarrow \gamma\gamma$ reads,

$$\Gamma(h_j \rightarrow \gamma\gamma) = \frac{G_F \alpha^2 m_h^3}{128 \sqrt{2} \pi^3} (|X_F^{\gamma\gamma} + X_W^{\gamma\gamma} + X_H^{\gamma\gamma}|^2), \quad (54)$$

where, noticing that for scalars the Y terms in [31] vanish,

$$X_F^{\gamma\gamma} = -\sum_f N_c^f 2a_j^f Q_f^2 \tau_f [1 + (1 - \tau_f) f(\tau_f)], \quad (55)$$

$$X_W^{\gamma\gamma} = C_j [2 + 3\tau_W + 3\tau_W(2 - \tau_W) f(\tau_W)], \quad (56)$$

$$X_H^{\gamma\gamma} = -\sum_{k=1}^2 \frac{\lambda_{h_j H_k^+ H_k^-} v^2}{2m_{H_k^\pm}^2} \tau_{jk}^\pm [1 - \tau_{jk}^\pm f(\tau_{jk}^\pm)]. \quad (57)$$

We used

$$\tau_f = 4m_f^2/m_{h_j}^2, \quad \tau_{jk}^\pm = 4m_{H_k^\pm}^2/m_{h_j}^2, \quad (58)$$

where m_f ($m_{H_k^\pm}$) is the mass of the relevant particle in the loop, while m_{h_j} is the mass of the decaying Higgs boson. The function $f(\tau)$ is defined in the Higgs Hunter's Guide [3],

$$f(\tau) = \begin{cases} \left[\sin^{-1}(\sqrt{1/\tau}) \right]^2, & \text{if } \tau \geq 1 \\ -\frac{1}{4} \left[\ln\left(\frac{1+\sqrt{1-\tau}}{1-\sqrt{1-\tau}}\right) - i\pi \right]^2, & \text{if } \tau < 1 \end{cases}, \quad (59)$$

and the couplings C_j and $\lambda_{h_j H_k^+ H_k^-}$ for this model are written in the Appendix. They were derived with the help of the software FeynMaster [32,33], that uses QGRAF [34], FeynRules [35,36] and FeynCalc [37,38] in an integrated way.

The decay into gluons can be obtained from the expression for the $\gamma\gamma$ decay,

$$\Gamma(h_j \rightarrow gg) = \frac{G_F \alpha_s^2 m_h^3}{64 \sqrt{2} \pi^3} (|X_F^{gg}|^2), \quad (60)$$

where

$$X_F^{gg} = -\sum_q 2a_j^q \tau_q [1 + (1 - \tau_q) f(\tau_q)], \quad (61)$$

and the sum runs only over quarks q .

For the 125 GeV scalar, the coupling modifiers, are calculated directly from the random angles generated and constrained to be within 2σ of the most recent ATLAS fit results, [39][Table 10]. Having chosen a specific production

and decay channel, the collider event rates can be conveniently described by the cross section ratios μ_{if}^h ,

$$\mu_{if}^h = \left(\frac{\sigma_i^{3\text{HDM}}(pp \rightarrow h)}{\sigma_i^{\text{SM}}(pp \rightarrow h)} \right) \left(\frac{\text{BR}^{3\text{HDM}}(h \rightarrow f)}{\text{BR}^{\text{SM}}(h \rightarrow f)} \right). \quad (62)$$

Starting from the collision of two protons, the relevant production mechanisms include: gluon fusion (ggH), vector boson fusion (VBF), associated production with a vector boson (VH, $V = W$ or Z), and associated production with a pair of top quarks (ttH). The SM cross section for the gluon fusion process is calculated using HIGLU [40], and for the other production mechanisms we use the results of Ref. [41]. Each of the 3HDM processes is obtained by rescaling the SM cross sections by the relevant relative couplings. As for the decay channels, we calculated the branching ratios for final states $f = WW, ZZ, b\bar{b}, \gamma\gamma$ and $\tau^+\tau^-$. Finally, we require that the μ_{if}^h for each individual initial state \times final state combination is consistent, within twice the total uncertainty, with the best-fit results presented in the most recent study of data collected at $\sqrt{s} = 13$ TeV with the ATLAS experiment [39][Fig. 5].

For the heavier neutral and charged scalars, we use HiggsBounds-5.9.1 in Ref. [18], where a list of all the relevant experimental analyses can be found. We allow for decays with off-shell scalar bosons, using the method explained in [42]. This is a generalization of the procedure used to evaluate the off-shell decays of the Higgs boson in the SM, (for instance $H \rightarrow W + W^*$, see [43]). Starting from the three body exact formula, and including the finite width in the off-shell propagator, one can show that the result reduces to an integration over the off-shell invariant mass of the two body formula multiplied by the propagator with appropriate factors. The inclusion of the finite width in the propagator makes that this expression merges smoothly with the on-shell case. We also consider the constraints coming from $b \rightarrow s\gamma$, as we explain in Secs. V and VI.

IV. DECAYS OF h_{125} IN THE Z_3 3HDM

In this section, we use the scan ranges defined in Eq. (21), pass them through all theoretical and experimental constraints, and we study the impact on the decays of the 125 GeV Higgs $h_1 = h_{125}$ found at LHC.

The contribution from the two charged scalars to the $h_{125} \rightarrow \gamma\gamma$ decay process is shown in Fig. 1. There are two interesting regimes. To the left (right) of the vertical line at coordinate zero, the two charged Higgs conspire to decrease (increase) the branching ratio into $\gamma\gamma$. Most of the points are on the left and correspond to a significant reduction of the decay width. However, there are indeed points on the right, which allow for an increase which could be up by 20%. We have also confirmed the existence of allowed results where the destructive interference between the two charged Higgs leads to a null $X_H^{\gamma\gamma}$, occurring when

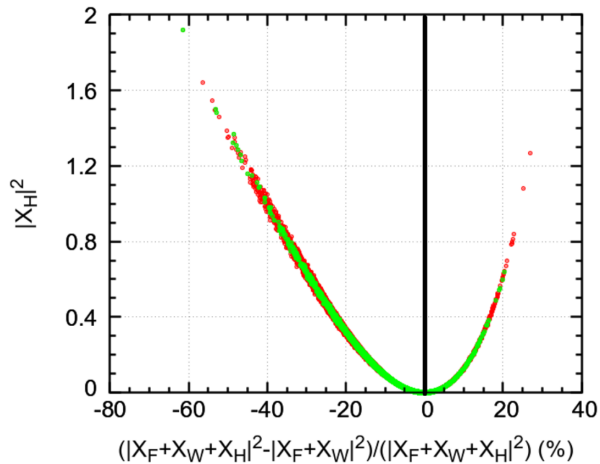


FIG. 1. Effect of the charged Higgs on the $h_{125} \rightarrow \gamma\gamma$ decay, with the definitions of Eq. (54). The green points passed all constraints including those coming from searches for extra scalars (incorporated in HB5), while the red points did not pass HB5 (see text for a discussion).

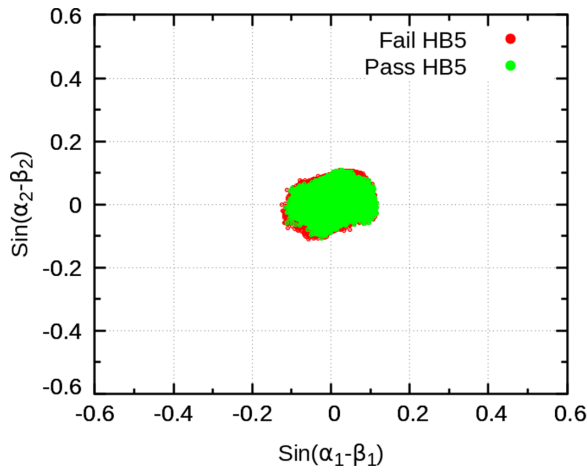


FIG. 2. Results of the simulation in the $\sin(\alpha_2 - \beta_2) - \sin(\alpha_1 - \beta_1)$ plane. The color code is as in Fig. 1. The point at (0,0) corresponds to the alignment limit.

the signs of the couplings $\lambda_{h_j H_1^+ H_1^-}$ and $\lambda_{h_j H_2^+ H_2^-}$ are opposite in Eq. (57). This means that, barring other constraints, the charged Higgs masses could be relatively light without contradicting the observed $h_{125} \rightarrow \gamma\gamma$, as long as their contributions to this decay canceled, as they may. The points in red pass all the theoretical constraints discussed in Sec. III as well as the signal strengths from ATLAS [39] [Table 10]. The green points are further constrained by the latest LHC results on the other Higgs scalars, incorporated in the latest version of HiggsBounds-5.9.1 (HB5).

The regions of Fig. 1 where $|X_H|^2$ is large, for which the charged Higgs provide a considerable contribution to the overall $h_{125} \rightarrow \gamma\gamma$ decay rate (the latter, still within current bounds) are only obtained for very fine tuned

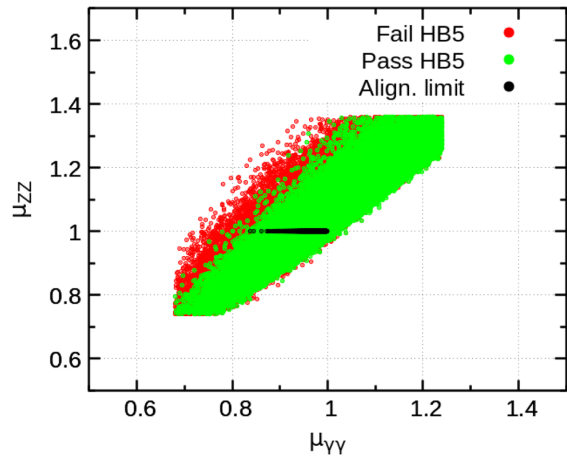


FIG. 3. Results in the $\mu_{ZZ} - \mu_{\gamma\gamma}$ plane for the gluon fusion production channel. The color code is as in Fig. 1. In addition, black points correspond to the perfect alignment limit of Eq. (73) below.

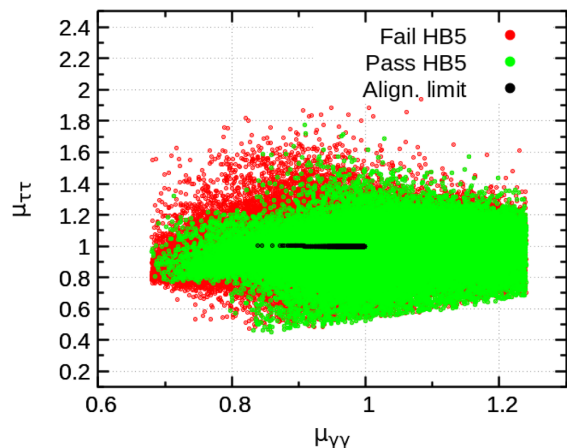


FIG. 4. Results in the $\mu_{\tau\tau} - \mu_{\gamma\gamma}$ plane for all production channels. The color code is as in Fig. 3.

points in parameter space with some charged Higgs mass below 200 GeV.⁵

The set of points that are consistent with all the bounds is now plotted in the $\sin(\alpha_2 - \beta_2) - \sin(\alpha_1 - \beta_1)$ plane as shown in Fig. 2. Comparing with the plot in the same plane shown in [13][Fig. 1], we find that the use of more recent experimental data for the simulated results leads to us being closer to the alignment limit, defined by $\alpha_1 = \beta_1$ and $\alpha_2 = \beta_2$. However, as illustrated here and in the following sections, points in parameter space slightly off the alignment limit exhibit physical properties which differ significantly from the exact alignment limit.⁶

⁵As we will see in Figs. 9–10 below, this is a very constrained (fine tuned) region.

⁶This difference will be even more striking when we consider the benchmark points discussed in Sec. VIII.

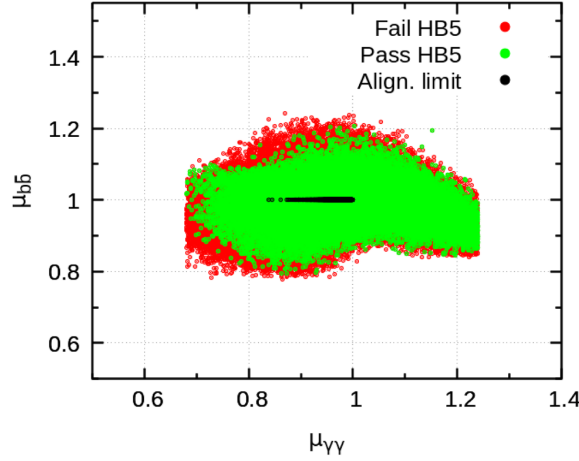


FIG. 5. Results in the $\mu_{bb} - \mu_{\gamma\gamma}$ plane for the gluon fusion production channel. The color code is as in Fig. 3.

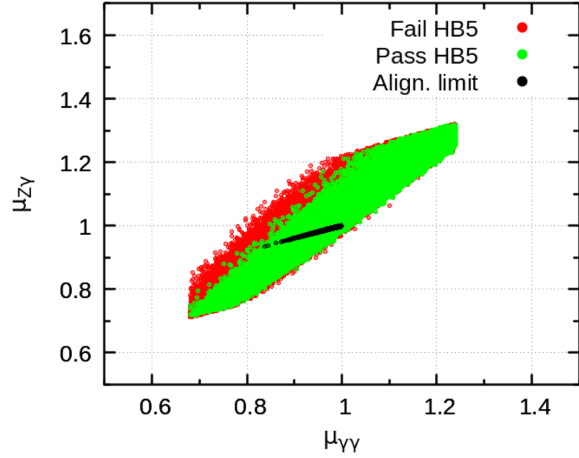


FIG. 6. Results in the $\mu_{Z\gamma} - \mu_{\gamma\gamma}$ plane for the gluon fusion production channel. The color code is as in Fig. 3.

To study the allowed regions for the signal strengths μ_{if}^h , we follow [31,44] and calculate each μ_{if}^h using all production channels. Our set of points is then shown in Figs. 3–6.

Figures 3–6 contain three interesting results. First, in these figures we compare the results before (red points) and after (green points) applying the LHC constraints on the heavier scalars incorporated in HB5. As discussed in the introduction (and explained in more detail in Sec. VI below), the new results from LHC constrain specially the $\tau\tau$ (Fig. 4) and bb (Fig. 5) channels. That is, the absence of $h_{2,3} \rightarrow \tau\tau, bb$ signals has the strongest impact in constraining on the model's parameter space. The difference between the red and green regions shows that one cannot ignore the constraints that LHC already places on the extra scalars (other than the 125 GeV Higgs). It is important to notice that, although such constraints come from observables related to the extra scalars, they do restrict

how much the properties of the 125 GeV Higgs can differ from the SM.

Second, Figs. 3–6 also contain in black the results obtained in the perfect alignment limit of Eq. (73) below [a black line close to the center of the figures, ending at the SM point (1,1)]. We see that points slightly off that limit yield predictions for the properties of the 125 GeV Higgs which differ markedly from those obtained in that exact limit.

Third, similar to the complex 2HDM analyzed by Fontes, Romão, and Silva in [31], there is a strong correlation between $\mu_{Z\gamma}$ and $\mu_{\gamma\gamma}$ in our type-Z model, as shown in Fig. 6. Such a correlation is also visible between μ_{ZZ} and $\mu_{\gamma\gamma}$ in Fig. 3. It is less apparent in correlations with $\tau^+\tau^-$ and bb , as shown in Figs. 4 and 5.

V. CALCULATION OF THE BR($B \rightarrow X_s\gamma$)

A. Introduction

It is well known that the experimental bounds on $B \rightarrow X_s\gamma$ place stringent restrictions on the parameter space of models with charged scalars [11,17,45–47]. Most notably, there is a bound on the mass of the only charged Higgs boson present in the type-II 2HDM which, at 95% CL (2σ), is according to [17]

$$m_{H^+} > 580 \text{ GeV}. \quad (63)$$

The exact value for this bound depends on both the theoretical approximations [48] and the experimental errors. The experimental average gives [49]

$$\text{BR}^{\text{exp}}(B \rightarrow X_s\gamma) = (3.32 \pm 0.15) \times 10^{-4}, \quad (64)$$

while the NNLO calculation within the SM yields [11,50]

$$\text{BR}^{\text{SM}}(B \rightarrow X_s\gamma) = (3.40 \pm 0.17) \times 10^{-4}, \quad (65)$$

with an error of about 5%.

As explained below, we will take an error of 2.5% around the central value of the calculation and, following [11], we consider 99% CL (3σ) for the experimental error:

$$2.87 \times 10^{-4} < \text{BR}(B \rightarrow X_s\gamma) < 3.77 \times 10^{-4}. \quad (66)$$

B. The calculation

We follow closely the calculation by Borzumati and Greub in Ref. [45]. There, the new contributions from the charged Higgs bosons are encoded in the Wilson coefficients,

$$\begin{aligned} C_7^{0,\text{eff}}(\mu_W) &= C_{7,\text{SM}}^{0,\text{eff}}(\mu_W) + |Y|^2 C_{7,\text{YY}}^{0,\text{eff}}(\mu_W) \\ &\quad + (XY^*) C_{7,\text{XY}}^{0,\text{eff}}(\mu_W), \end{aligned} \quad (67a)$$

$$C_8^{0,\text{eff}}(\mu_W) = C_{8,\text{SM}}^{0,\text{eff}}(\mu_W) + |Y|^2 C_{8,\text{YY}}^{0,\text{eff}}(\mu_W) + (XY^*) C_{8,\text{XY}}^{0,\text{eff}}(\mu_W), \quad (67b)$$

$$C_4^{1,\text{eff}}(\mu_W) = E_0(x) + \frac{2}{3} \log\left(\frac{\mu_W^2}{M_W^2}\right) + |Y|^2 E_H(y), \quad (67c)$$

$$C_7^{1,\text{eff}}(\mu_W) = C_{7,\text{SM}}^{1,\text{eff}}(\mu_W) + |Y|^2 C_{7,\text{YY}}^{1,\text{eff}}(\mu_W) + (XY^*) C_{7,\text{XY}}^{1,\text{eff}}(\mu_W), \quad (67d)$$

$$C_8^{1,\text{eff}}(\mu_W) = C_{8,\text{SM}}^{1,\text{eff}}(\mu_W) + |Y|^2 C_{8,\text{YY}}^{1,\text{eff}}(\mu_W) + (XY^*) C_{8,\text{XY}}^{1,\text{eff}}(\mu_W), \quad (67e)$$

where we are using the notation in Ref. [45] which should be consulted for the definitions and also for the procedure used in evolving the coefficients to the scale $\mu_b = m_b$. The dependence on the charged Higgs mass appears because the functions $C_{i,\text{YY}}^{0,\text{eff}}$, $C_{i,\text{XY}}^{0,\text{eff}}$, $C_{i,\text{YY}}^{1,\text{eff}}$, and $C_{i,\text{XY}}^{1,\text{eff}}$ depend on $y = m_i^2/m_{H^\pm}^2$, while the SM coefficients depend on $x = m_i^2/M_W^2$.

For models with multiple charged Higgs there is one contribution (and one parameter y_k) for each particle. A model with two charged Higgs is discussed in [11,12], with interesting earlier work highlighting the possible cancellation between the two charged Higgs contributions appearing in Refs. [51,52]. We obtain, for example,

$$C_7^{1,\text{eff}}(\mu_W) = C_{7,\text{SM}}^{1,\text{eff}}(\mu_W) + |Y_1|^2 C_{7,\text{YY}}^{1,\text{eff}}(\mu_W, y_1) + |Y_2|^2 C_{7,\text{YY}}^{1,\text{eff}}(\mu_W, y_2) + (X_1 Y_1^*) C_{7,\text{XY}}^{1,\text{eff}}(\mu_W, y_1) + (X_2 Y_2^*) C_{7,\text{XY}}^{1,\text{eff}}(\mu_W, y_2), \quad (68)$$

where we wrote explicitly the dependence on the charged Higgs masses,

$$y_1 = \frac{m_t^2}{m_{H_1^\pm}^2}, \quad y_2 = \frac{m_t^2}{m_{H_2^\pm}^2}, \quad (69)$$

and used

$$X_1 = -\frac{\mathbf{Q}_{22}}{\cos\beta_2 \sin\beta_1}, \quad Y_1 = \frac{\mathbf{Q}_{23}}{\sin\beta_2}, \\ X_2 = -\frac{\mathbf{Q}_{32}}{\cos\beta_2 \sin\beta_1}, \quad Y_2 = \frac{\mathbf{Q}_{33}}{\sin\beta_2}. \quad (70)$$

We took the input parameters from Ref. [45] except for $\alpha_s(M_Z)$, m_t , M_Z , M_W , that were updated to the most recent values of the Particle Data Group [53]⁷:

⁷If we use exclusively the input values of Ref. [45], we reproduce their SM results. We are extremely grateful to C. Greub for discussions and for providing us with the original code used in [45], utilized to cross check our independent calculations.

$$\alpha_s(M_Z) = 0.1179 \pm 0.0010, \quad m_t = 172.76 \pm 0.3 \text{ GeV}, \quad (71a)$$

$$m_c/m_b = 0.29 \pm 0.02, \quad m_b - m_c = 3.39 \pm 0.04 \text{ GeV}, \quad (71b)$$

$$\alpha_{em}^{-1} = 137.036, \quad |V_{ts}^* V_{tb}/V_{cb}|^2 = 0.95 \pm 0.03, \quad (71c)$$

$$\text{BR}_{SL} = 0.1049 \pm 0.0046. \quad (71d)$$

where BR_{SL} is the measured semileptonic branching ratio of the B meson (see Ref. [45]).

VI. IMPACT OF $b \rightarrow s\gamma$ AND HB5 ON THE Z_3 3HDM PARAMETER SPACE

As mentioned, Ref. [17] points out that current constraints on $b \rightarrow s\gamma$ applied to the type II 2HDM force the charged Higgs to have a mass above 580 GeV. Reference [15] makes the important point that this is no longer the case for the Z_3 3HDM, where one of the charged Higgs can have a relatively low mass. This possibility is shown on the relevant Fig. 2 of Ref. [15], where the parameters are fixed as

$$\tan\beta_1 = 10, \quad \tan\beta_2 = 2, \quad \gamma_2 = \frac{\pi}{6}, \frac{\pi}{4}, \frac{\pi}{3}, \quad (72)$$

while imposing

$$m_{h_2} = m_{A_1} = m_{H_1^\pm}, \quad m_{h_3} = m_{A_2} = m_{H_2^\pm}, \\ \alpha_1 = \beta_1, \quad \alpha_2 = \beta_2, \quad \gamma_1 = \gamma_2 = -\alpha_3. \quad (73)$$

Eq. (73) is dubbed the perfect alignment limit. With the choice of Eqs. (72)–(73), the bounds from the decays of the 125 GeV Higgs, implemented using signal strengths from ATLAS [39][Table 10], are easily satisfied because we are at the alignment limit. However the same is not true for current bounds on heavier scalars. Indeed, every single point in the range (72)–(73) is excluded by the data from searches into heavier states and incorporated into HB5. We will now show that enlarging the scanning region beyond the perfect alignment of Eqs. (72)–(73) will yield points which are consistent with all available data.

A. Enlarging the scanning region

We discovered that the situation just described is a consequence of the small range chosen for γ_2 . To illustrate this, we kept the other conditions in Eqs. (72)–(73), but allowed for

$$\gamma_2 \in [-\pi/2, \pi/2], \quad (74)$$

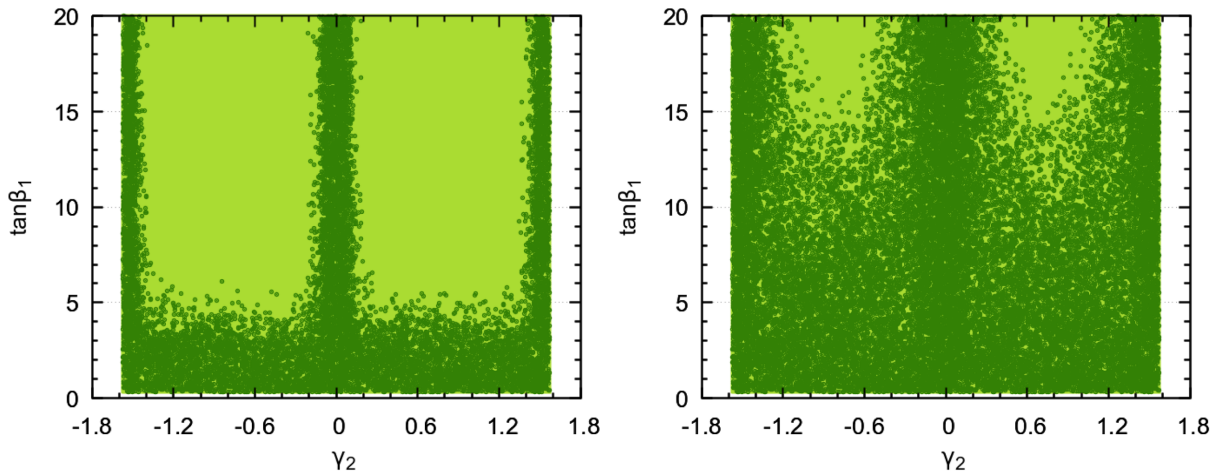


FIG. 7. Enlarging the scanning region, taking $\gamma_2 \in [-\pi/2, \pi/2]$ and varying β_1 . All other conditions in Eqs. (72)–(73) were kept. The dark green points passed all constraints including the constraints from searches of extra scalars incorporated into HB5, while the light green points did not pass HB5. Left panel: All points passing HiggsBounds-5.9.1. Right panel: All points passing HiggsBounds-5.7.1. See text for a discussion on the physics behind the difference.

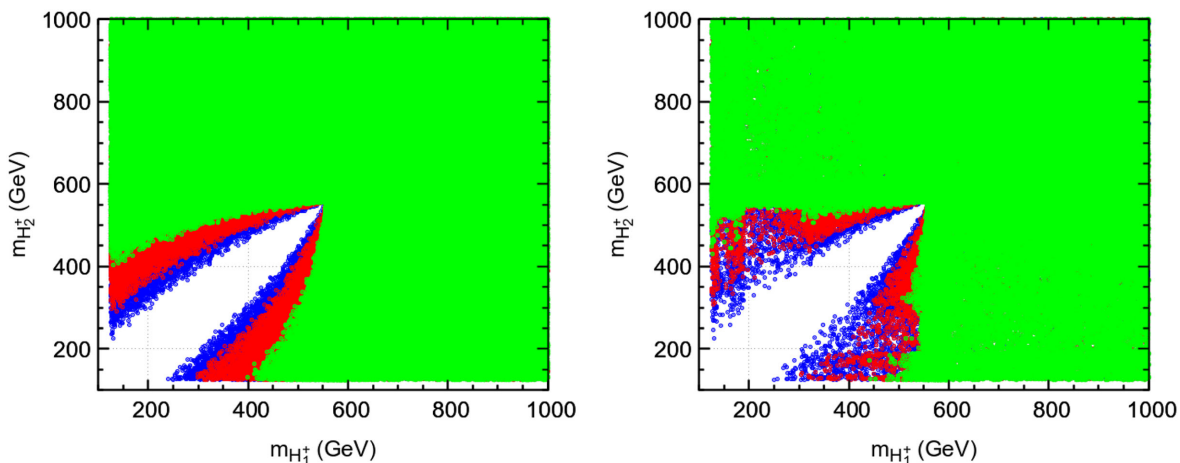


FIG. 8. All points satisfy Eq. (73). Left panel: All points passed all constraints except for HB5. The blue points satisfy Eq. (75). The red points are for $\tan \beta_{1,2} > 0.5$ and the green points are for $\tan \beta_{1,2} > 1$. Right panel: same color code as in the left panel but only showing points surviving after requiring HB5, which implements the LHC searches for heavier scalars.

and (for Fig. 7) also varied $\tan \beta_1$. The points which survive HiggsBounds-5.9.1 are shown in dark green on the left panel of Fig. 7.

The allowed points for $\tan \beta_1 = 10$ are concentrated around $\gamma_2 = 0, \pm\pi/2$, thus excluding $\gamma_2 = \pi/6, \pi/4, \pi/3$. Taking the interval in Eq. (74) one can indeed find regions of good points.⁸

To understand the physics behind this finding, we have compared the latest version HiggsBounds-5.9.1 on the left panel of Fig. 7, with the previous HiggsBounds-5.7.1 shown on the right panel. For that case there are many points allowed for all values of γ_2 , even for $\tan \beta_1 = 10$. We have found that this is due to the recent bounds on $h_{2,3} \rightarrow \tau^+ \tau^-$ decay

⁸This is true regardless of whether or not we vary β_1 , as long as we enlarge the scanning region of γ_2 .

in Ref. [19], included in HiggsBounds-5.9.1 but not in HiggsBounds-5.7.1, which used the previous bounds [54,55].⁹ To better illuminate this point, we study $\sigma(pp \rightarrow h_2) \times \text{BR}(h_2 \rightarrow \tau\tau)$ in detail in Appendix B.

B. The effect of $\tan \beta$'s

In the last section we saw that while maintaining the main features of Eqs. (72)–(73), but enlarging the range of variation of γ_2 , we could find points allowed by all current experimental constraints. Here we exploit the variation of both $\tan \beta$'s in the range

⁹In Ref. [15] the strong constraints from neutral scalar decays into $\tau\tau$ still seemed to allow points with the choices in Eqs. (72)–(73).

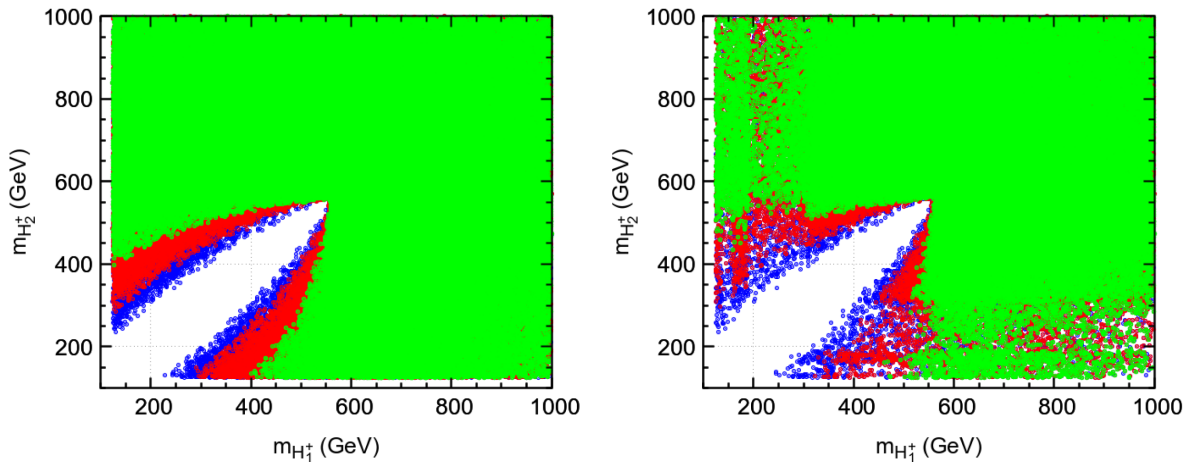


FIG. 9. All points are within 1% of the perfect alignment of Eq. (73). Left panel: all points passed all constraints except for HB5. The blue points satisfy Eq. (75). The red points are for $\tan\beta_{1,2} > 0.5$ and the green points are for $\tan\beta_{1,2} > 1$. Right panel: same color code as in the left panel but only showing points surviving after requiring HB5, which implements the LHC searches for heavier scalars.

$$\tan\beta_{1,2} \in [10^{-0.5}, 10], \quad (75)$$

subject to the condition of perturbativity of the Yukawa couplings in Eq. (52). The result is shown in Fig. 8.

We see that by varying the range of $\tan\beta$'s we can have smaller masses for the charged Higgs bosons. For $\tan\beta < 1$ it is even possible to have both charged Higgs with masses below 400 GeV; an important new result.

VII. GOING BEYOND PERFECT ALIGNMENT

In our initial scan leading to Figs. 1–6 we varied the parameters in the ranges in Eq. (21) without any additional constraint. However, we found out that very few points survived and those were not too far away from the alignment condition of Eq. (73). So another strategy can be to scan points that differ from the perfect alignment of Eq. (73) by 1% or 10%. Let us clarify what we mean by this. Take the 1% case. We scan $\beta_1, \beta_2, \gamma_1$ and m_{h_2}, m_{h_3} in the intervals of Eq. (21), but for the other parameters instead of perfect alignment as in Eq. (73) we consider

$$\alpha_1 \in [0.99\beta_1, 1.01\beta_1], \quad \alpha_2 \in [0.99\beta_2, 1.01\beta_2] \quad (76)$$

$$m_{A_1} \in [0.99m_{h_2}, 1.01m_{h_2}], \quad m_{A_2} \in [0.99m_{h_3}, 1.01m_{h_3}] \quad (77)$$

and similarly for the other parameters.

In Fig. 9 we show the results for the case when we allow the parameters to differ 1% from the perfect alignment limit.

Next we considered the case when the difference for perfect alignment was between 1% and 10%. This is shown in Fig. 10.

We note two issues. The points in Fig. 10 (further away from alignment) are much harder to generate than the

points in Fig. 9 (closer to the alignment limit). Also, we note that the figures are almost identical, meaning that the impact of all current theoretical and experimental constraints allows exactly the same structure on the $m_{H_1^\pm} - m_{H_2^\pm}$ plane, whether one is within 1% of perfect alignment, or between 1% and 10%. But the points further away from alignment (shown in Fig. 10) do allow for qualitatively different predictions, as we saw in Sec. IV and as we will discuss in Sec. VIII below, in the study of relevant benchmark points. We conclude that imposing perfect alignment is too constraining and does not cover all the interesting features of the \mathbb{Z}_3 3HDM.

A. Unusual signals of charged scalars

As we have seen, the contributions of the two charged scalars can exhibit large cancellations in the decays $h \rightarrow \gamma\gamma$ and $B \rightarrow X_s\gamma$.¹⁰ For some choices of parameter space, it is even possible that there are cancellations in both decays simultaneously. This is illustrated in Fig. 11.

Such charged scalars would, thus, be difficult to probe indirectly.

Notice that points with exact alignment, in cyan in Fig. 11, do not allow for cancellation in $h \rightarrow \gamma\gamma$; but alignment with 1% already does.

Most points within the blue box close to (0,0) have H_2^\pm decays into quarks or leptons, which are being sought at LHC. But there are points which could also be difficult to probe directly with such common searches, even though one or both charged scalars might have relatively small masses. Indeed, one can find fine-tuned points in parameter space

¹⁰For 3HDMs, the cancellation can be exact in $B \rightarrow X_s\gamma$ because there are two charged components of Higgs doublets feeding the two physical charged Higgs states. This is no longer the case in the Zee model, with two Higgs doublets and one charged scalar singlet [56].

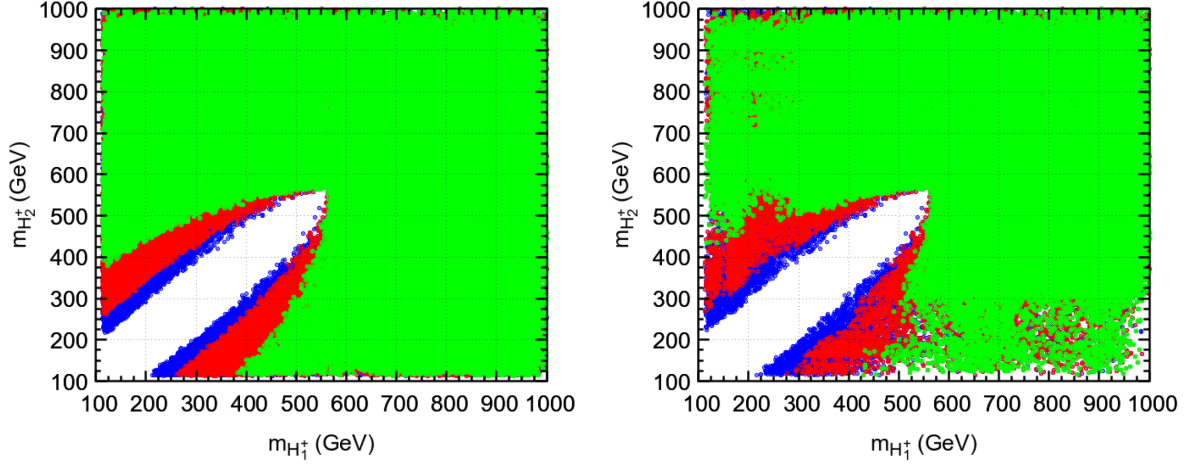


FIG. 10. All points are within 1%-10% of the perfect alignment of Eq. (73). Left panel: all points passed all constraints except for HB5. The blue points satisfy Eq. (75). The red points are for $\tan \beta_{1,2} > 0.5$ and the green points are for $\tan \beta_{1,2} > 1$. Right panel: same color code as in the left panel but only showing points surviving after requiring HB5, which implements the LHC searches for heavier scalars.

where the H_2^+ does not decay primordially into quarks or leptons, but rather as $H_2^+ \rightarrow H_1^+ h_j$ with $h_j = h_1, h_2, A_1$. We propose that such decays be actively searched for at LHC's next run. To aid in that experimental endeavor, we present some benchmark points (BP) in the next section.

VIII. ILLUSTRATIVE BENCHMARK POINTS

This section is devoted to some benchmark points/lines, with features which may prove useful for the experimental searches.

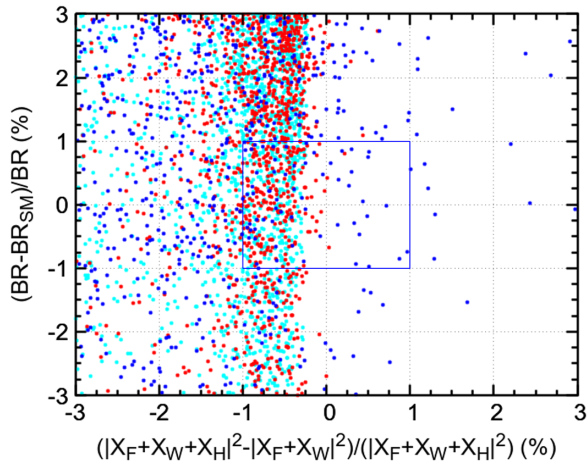


FIG. 11. Points with significant approximate cancellation of the charged Higgs contributions to both $h \rightarrow \gamma\gamma$ (horizontal axis) and $B \rightarrow X_s \gamma$ (vertical), which pass all theoretical and experimental bounds, including HB5. Color code: cyan is perfect alignment, red means alignment within 1%, and blue means alignment within 10%. The blue box guides the eye to those points closest to (0,0).

There has been a recent interest in the literature for unusual decays of the charged Higgs [57], specially those in which the charged Higgs decays to $W^+ h_i$ where h_i is any of the scalars or pseudoscalars in the model.

We have performed a search in our large datasets and found many points where $\text{BR}(H_1^+ \rightarrow W^+ + h_{125})$

TABLE I. Benchmark points for the type Z Z_3 -3HDM.

Type-Z	BP1	BP2	BP3
m_{h_2}	419.00	494.60	486.26
m_{h_3}	799.60	850.88	694.44
m_{A_1}	413.80	483.96	513.46
m_{A_2}	763.15	806.44	647.56
$m_{H_1^\pm}$	396.13	477.63	506.36
$m_{H_2^\pm}$	752.81	843.034	654.77
(m_{12}^2)	-8350	-31768	-19562
(m_{13}^2)	-83278	-80800	-63134
(m_{23}^2)	-231428	-232361	-197019
α_1	1.289	1.343	1.328
α_2	0.5419	0.4406	0.7119
α_3	0.00543	-0.00299	0.01136
γ_1	-0.00503	0.00322	-0.01078
γ_2	-0.00504	0.00301	-0.01011
β_1	1.192	1.263	1.231
β_2	0.5077	0.4311	0.7351
$\text{BR}(H_1^+ \rightarrow \nu_\tau + \tau^+)$	0.0688	0.0790	0.0784
$\text{BR}(H_1^+ \rightarrow t + \bar{b})$	0.0383	0.0197	0.0358
$\text{BR}(H_1^+ \rightarrow W^+ h_1)$	0.8926	0.9011	0.8855
$\text{BR}(H_2^+ \rightarrow t + \bar{b})$	0.9970	0.9995	0.9965
$\text{BR}(H_2^+ \rightarrow W^+ h_1)$	0.0012	0.0001	0.0009
$\text{BR}(H_2^+ \rightarrow W^+ h_2)$	0.0007	0.0003	0.0006

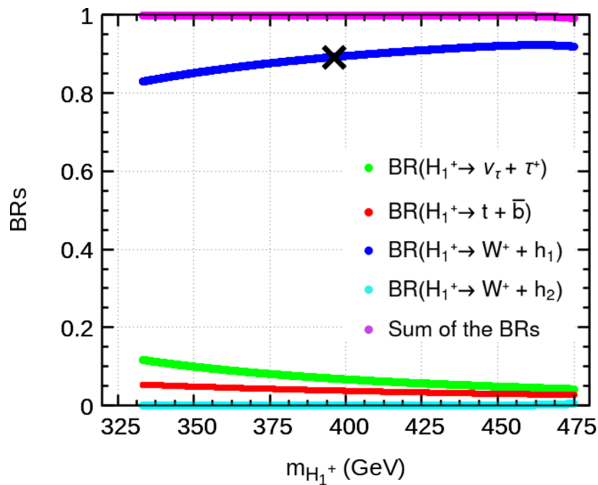


FIG. 12. Most important BR's for BP1. The black cross corresponds to the original BP in Table I.

was larger than 80%. From those we selected three benchmark points (BP) that we list in Table I. For each of these BP we let the mass of the H_1^+ vary, leaving all the other parameters fixed, obtaining benchmark lines. All these points verify all the constraints, including those from HiggsBounds-5.9.1. These BP, shown in Figs. 12 and 13, all have the characteristic that the dominant decay of the charged H_1^+ is not in the tb channel, but in W^+h_{125} , which makes these interesting and deserving to be searched at the LHC.

Notice that, for these BP, the other charged Higgs decays 100% in tb . For BP2 the decay $H_1^+ \rightarrow W^+A_1$ opens up when the mass of the H_1^+ is such that $m_{H_1^+} > M_W + m_{A_1}$ explaining the decrease in our preferred branching ratio (see left panel of Fig. 13). The same happens for the channel $H_1^+ \rightarrow W^+h_2$ for BP3 as can be seen in the right panel of Fig. 13.

Notice that the interesting channels studied in this section are completely forbidden in the alignment limit

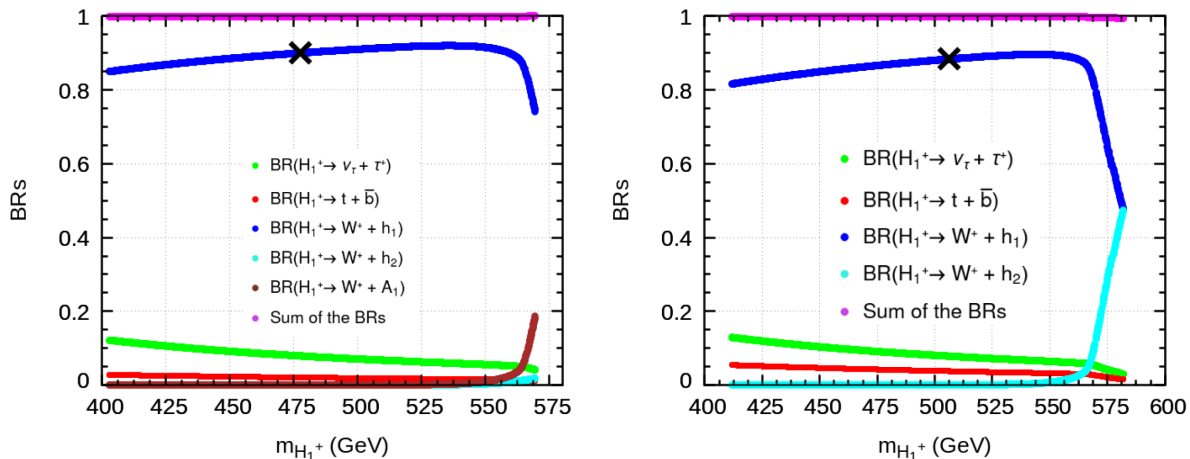


FIG. 13. Most important BR's for BP2 (left panel) and BP3 (right panel). The black cross corresponds to the original BP in Table I.

of $\alpha_1 = \beta_1, \alpha_2 = \beta_2$. For example, the coupling $H_1^+ W^- h_1$ is proportional to

$$\begin{aligned}
 g_{h_1 H_1^+ W^-} &= \mathbf{R}_{11} \mathbf{Q}_{21} + \mathbf{R}_{12} \mathbf{Q}_{22} + \mathbf{R}_{13} \mathbf{Q}_{23} \\
 &= \sin \gamma_2 [-\sin(\alpha_2 - \beta_2) \\
 &\quad + \cos \alpha_2 \sin \beta_2 (\cos(\alpha_1 - \beta_1) - 1)] \\
 &\quad + \cos \gamma_2 \cos \alpha_2 \sin(\alpha_1 - \beta_1), \quad (78)
 \end{aligned}$$

and this obviously vanishes in the alignment limit. Thus, it is crucial to go beyond exact alignment when studying the physical implications of (and direct experimental searches for) multi scalar models.

IX. CONCLUSIONS

Multi-Higgs models with $N \geq 3$ allow for the possibility that all fermions of a given charge couple exclusively to one dedicated scalar. These are known as type-Z models, and constitute a fifth alternative beyond the four natural flavor conservation models allowed in the 2HDM. We investigate the current bounds on the type-Z 3HDM imposed by a \mathbb{Z}_3 symmetry. We perform an up-to-date analysis including the latest data for the 125 GeV Higgs [39], bounds on new scalars through the HiggsBounds-5.9.1 code [18], and the theoretical constraints.

We use the theoretical bounds from unitarity [16] and BFB; the latter developed here for the first time. We stress the importance of using the most recent LHC bounds, which constrain severely the allowed parameter space. In particular, we show that bounds from $h_2 \rightarrow \tau^+ \tau^-$ alter significantly some results in the literature [15]. This is clearly visible in our Fig. 7 and Fig. 14. Moreover, we also stress the fact that interesting physical observables may differ significantly when one considers situations close to the alignment limit, versus adopting the exact alignment limit. Indeed, current LHC bounds on the productions and

branching ratios of the 125 GeV neutral scalar force the measured couplings to lie close to those obtained for the SM Higgs. Nevertheless, forcing those couplings to match *exactly* those in the SM is too constraining on the parameter space and precludes much of the interesting new features that the Z_3 3HDM has. This is particularly true for the signal strengths shown in Figs. 3–6, that can deviate from exact alignment while being still compatible with all the experimental data, and for the study of benchmark points in Sec. VIII.

We look at the constraints allowed by current data on the 125 GeV Higgs decays, including a detailed look at $h \rightarrow \gamma\gamma$ and its correlations with the other decays. We point out the possibility that the contributions from the two charged scalars might cancel in $h \rightarrow \gamma\gamma$. This is also possible in $B \rightarrow X_s \gamma$, and we explore explicitly how this allows for lower masses for the charged scalars. In particular, we found that for $\tan\beta < 1$ it is even possible to have both charged Higgs with masses below 400 GeV. We provide illustrative benchmark points to aid in experimental searches. By comparing the constraints from HiggsBounds-5.7.1 and the newer HiggsBounds-5.9.1 (which reflect an improvement in the LHC searches for extra scalars) we highlight the importance that the next LHC run will have in further constraining this model, or perhaps, finally uncovering new physics in the scalar sector.

ACKNOWLEDGMENTS

We are very grateful to D. Das for detailed discussions regarding his Ref. [15]. We are also very grateful to C. Greub for detailed discussions regarding his Refs. [45,46]. J. P. S. is grateful to Z. Ligeti for discussions.

This work is supported in part by the Portuguese Fundação para a Ciência e Tecnologia (FCT) under Contracts No. CERN/FIS-PAR/0008/2019, No. PTDC/FIS-PAR/29436/2017, No. UIDB/00777/2020, and No. UIDP/00777/2020; these projects are partially funded through Programa Operacional Ciência, Tecnologia, Inovação (POCTI) (FEDER), Programa Operacional Factores de Competitividade (COMPETE), Quadro de Referência Estratégico Nacional (QREN), and the EU.

APPENDIX A: SOME IMPORTANT COUPLINGS

This Appendix is devoted to some important couplings for the Z_3 3HDM used in our calculations. In our conventions these couplings include the i from the Feynman rules. These couplings were derived with the help of the software FeynMaster [32,33].

1. Scalar couplings to W^\pm bosons

We find for the neutral scalar couplings to W^+W^- ,

$$[h_j, W_\nu^+, W_\rho^-] = igM_W g_{\nu\rho} (R_{j1}\hat{v}_1 + R_{j2}\hat{v}_2 + R_{j3}\hat{v}_3) \quad (\text{A1})$$

Thus,

$$C_j = R_{j1}\hat{v}_1 + R_{j2}\hat{v}_2 + R_{j3}\hat{v}_3, \quad (\text{A2})$$

is to be used in Eq. (56).

2. Scalar couplings to charged Higgs

The couplings of the scalars h_j with $j = 1, 2, 3$ to the charged Higgs H_{k-1}^\mp, H_{l-1}^\pm where $k, l = 2, 3$ (we do not consider here the charged Goldstone) are,

$$\begin{aligned} [h_j, H_{k'}^\mp, H_{l'}^\pm] &= \frac{-i}{2} v [4\lambda_1 Q_{k1} Q_{l1} R_{j1} \hat{v}_1 + 2\lambda_5 Q_{k3} Q_{l3} R_{j1} \hat{v}_1 + \lambda_7 Q_{k2} Q_{l1} R_{j2} \hat{v}_1 + \lambda_{10} Q_{k3} Q_{l1} R_{j2} \hat{v}_1 + \lambda_7 Q_{k1} Q_{l2} R_{j2} \hat{v}_1 \\ &\quad + \lambda_{11} Q_{k3} Q_{l2} R_{j2} \hat{v}_1 + \lambda_{10} Q_{k1} Q_{l3} R_{j2} \hat{v}_1 + \lambda_{11} Q_{k2} Q_{l3} R_{j2} \hat{v}_1 + \lambda_{10} Q_{k2} Q_{l1} R_{j3} \hat{v}_1 + \lambda_8 Q_{k3} Q_{l1} R_{j3} \hat{v}_1 \\ &\quad + \lambda_{10} Q_{k1} Q_{l2} R_{j3} \hat{v}_1 + \lambda_{12} Q_{k3} Q_{l2} R_{j3} \hat{v}_1 + \lambda_8 Q_{k1} Q_{l3} R_{j3} \hat{v}_1 + \lambda_{12} Q_{k2} Q_{l3} R_{j3} \hat{v}_1 + \lambda_7 Q_{k2} Q_{l1} R_{j1} \hat{v}_2 \\ &\quad + \lambda_{10} Q_{k3} Q_{l1} R_{j1} \hat{v}_2 + \lambda_7 Q_{k1} Q_{l2} R_{j1} \hat{v}_2 + \lambda_{11} Q_{k3} Q_{l2} R_{j1} \hat{v}_2 + \lambda_{10} Q_{k1} Q_{l3} R_{j1} \hat{v}_2 + \lambda_{11} Q_{k2} Q_{l3} R_{j1} \hat{v}_2 \\ &\quad + 4\lambda_2 Q_{k2} Q_{l2} R_{j2} \hat{v}_2 + 2\lambda_6 Q_{k3} Q_{l3} R_{j2} \hat{v}_2 + \lambda_{11} Q_{k2} Q_{l1} R_{j3} \hat{v}_2 + \lambda_{12} Q_{k3} Q_{l1} R_{j3} \hat{v}_2 + \lambda_{11} Q_{k1} Q_{l2} R_{j3} \hat{v}_2 \\ &\quad + \lambda_9 Q_{k3} Q_{l2} R_{j3} \hat{v}_2 + \lambda_{12} Q_{k1} Q_{l3} R_{j3} \hat{v}_2 + \lambda_9 Q_{22} Q_{l3} R_{j3} \hat{v}_2 + 2\lambda_4 (Q_{22} Q_{l2} R_{j1} \hat{v}_1 + Q_{k1} Q_{l1} R_{j2} \hat{v}_2) \\ &\quad + \lambda_{10} Q_{22} Q_{l1} R_{j1} \hat{v}_3 + \lambda_8 Q_{k3} Q_{l1} R_{j1} \hat{v}_3 + \lambda_{10} Q_{k1} Q_{l2} R_{j1} \hat{v}_3 + \lambda_{12} Q_{k3} Q_{l2} R_{j1} \hat{v}_3 + \lambda_8 Q_{k1} Q_{l3} R_{j1} \hat{v}_3 \\ &\quad + \lambda_{12} Q_{22} Q_{l3} R_{j1} \hat{v}_3 + \lambda_{11} Q_{22} Q_{l1} R_{j2} \hat{v}_3 + \lambda_{12} Q_{k3} Q_{l1} R_{j2} \hat{v}_3 + \lambda_{11} Q_{k1} Q_{l2} R_{j2} \hat{v}_3 + \lambda_9 Q_{k3} Q_{l2} R_{j2} \hat{v}_3 \\ &\quad + \lambda_{12} Q_{k1} Q_{l3} R_{j2} \hat{v}_3 + \lambda_9 Q_{22} Q_{l3} R_{j2} \hat{v}_3 + 2\lambda_5 Q_{k1} Q_{l1} R_{j3} \hat{v}_3 + 2\lambda_6 Q_{22} Q_{l2} R_{j3} \hat{v}_3 + 4\lambda_3 Q_{k3} Q_{l3} R_{j3} \hat{v}_3] \\ &\equiv iv\lambda_{h_j, H_{k'}^\mp, H_{l'}^\pm}, \end{aligned} \quad (\text{A3})$$

where we have defined $k' \equiv k - 1$, $l' \equiv l - 1$ with $j = 1, 2, 3$ and $k, l = 2, 3$. Recall that $\hat{v}_k = v_k/v$. The coupling $\lambda_{h_j, H_{k'}^\mp, H_{l'}^\pm}$ is to be used in Eq. (57).

3. Pseudoscalar couplings to charged Higgs

The couplings of the pseudoscalars $A_{j'}$ with $j' = j - 1$ and $j = 2, 3$ (we do not consider the coupling of the neutral Goldstone) are

$$\begin{aligned}
[A_{j'}, H_1^\mp, H_2^\pm] = & \pm \frac{1}{2} v [\lambda_8 P_{j3} Q_{23} Q_{31} \hat{v}_1 + \lambda_{11} P_{j2} Q_{23} Q_{32} \hat{v}_1 - \lambda_{12} P_{j3} Q_{23} Q_{32} \hat{v}_1 - \lambda_8 P_{j3} Q_{21} Q_{33} \hat{v}_1 - \lambda_{11} P_{j2} Q_{22} Q_{33} \hat{v}_1 \\
& + \lambda_{12} P_{j3} Q_{22} Q_{33} \hat{v}_1 + \lambda_{11} P_{j3} Q_{22} Q_{31} \hat{v}_2 - \lambda_{12} P_{j3} Q_{23} Q_{31} \hat{v}_2 - \lambda_{11} P_{j3} Q_{21} Q_{32} \hat{v}_2 - \lambda_{11} P_{j1} Q_{23} Q_{32} \hat{v}_2 \\
& + \lambda_9 P_{j3} Q_{23} Q_{32} \hat{v}_2 + \lambda_{12} P_{j3} Q_{21} Q_{33} \hat{v}_2 + \lambda_{11} P_{j1} Q_{22} Q_{33} \hat{v}_2 - \lambda_9 P_{j3} Q_{22} Q_{33} \hat{v}_2 \\
& + \lambda_7 (Q_{22} Q_{31} - Q_{21} Q_{32}) (P_{j2} \hat{v}_1 - P_{j1} \hat{v}_2) - \lambda_{11} P_{j2} Q_{22} Q_{31} \hat{v}_3 - \lambda_8 P_{j1} Q_{23} Q_{31} \hat{v}_3 + \lambda_{12} P_{j2} Q_{23} Q_{31} \hat{v}_3 \\
& + \lambda_{11} P_{j2} Q_{21} Q_{32} \hat{v}_3 + \lambda_{12} P_{j1} Q_{23} Q_{32} \hat{v}_3 - \lambda_9 P_{j2} Q_{23} Q_{32} \hat{v}_3 + \lambda_8 P_{j1} Q_{21} Q_{33} \hat{v}_3 - \lambda_{12} P_{j2} Q_{21} Q_{33} \hat{v}_3 \\
& - \lambda_{12} P_{j1} Q_{22} Q_{33} \hat{v}_3 + \lambda_9 P_{j2} Q_{22} Q_{33} \hat{v}_3 + \lambda_{10} (-P_{j3} Q_{22} Q_{31} \hat{v}_1 - P_{j2} Q_{23} Q_{31} \hat{v}_1 + P_{j3} Q_{21} Q_{32} \hat{v}_1 \\
& + P_{j2} Q_{21} Q_{33} \hat{v}_1 + P_{j1} Q_{23} Q_{31} \hat{v}_2 - P_{j1} Q_{21} Q_{33} \hat{v}_2 + P_{j1} Q_{22} Q_{31} \hat{v}_3 - P_{j1} Q_{21} Q_{32} \hat{v}_3)], \\
\equiv & v \lambda_{A_j H_1^\mp H_2^\pm},
\end{aligned} \tag{A4}$$

for $j' = j - 1$ and $j = 2, 3$. Note that $\lambda_{A_j H_1^\mp H_2^\pm}$ and $\lambda_{A_j H_2^\mp H_2^\pm}$ vanish.

APPENDIX B: DETAILED STUDY OF $\sigma(pp \rightarrow h_2) \times \text{BR}(h_2 \rightarrow \tau\tau)$

This Appendix is devoted to a detailed explanation of the two results found in Sec. VI A. Recall that in the beginning of Sec. VI we learned that the constraints that LHC has placed on extra scalars (and encoded into HB5) already excludes *all* of the points defined by Eqs. (72)–(73). In Sec. VI A we learned that: (i) there are strong constraints placed on the γ_2 allowed region; and (ii) those constraints are mainly due to bounds on $h_{2,3} \rightarrow \tau^+ \tau^-$ decay, whose consequences on the \mathbb{Z}_3 parameter space improved noticeably when changing from the old results of Refs. [54,55], included in HiggsBounds-5.7.1, into the new results of Ref. [19], included in HiggsBounds-5.9.1. To better illuminate

this issue, we show $\sigma(pp \rightarrow h_2) \times \text{BR}(h_2 \rightarrow \tau\tau)$ versus m_{h_2} in Fig. 14. In this figure, the parameters are as in Eqs. (72)–(73), except that $\gamma_2 \in [-\pi/2, \pi/2]$. Points in cyan are points that pass all constraints before HIGGSBOUNDS. In light green are the points in the restricted interval $\gamma_2 \in [\pi/6, \pi/3]$. In the left panel points in dark green are those who survived after HiggsBounds-5.7.1. In the right panel we have the same situation but now we used HiggsBounds-5.9.1. We see that there were good points in the restricted interval $\gamma_2 \in [\pi/6, \pi/3]$ in the left panel, but they disappeared with the newer version HiggsBounds-5.9.1. We have confirmed that similar plots can be obtained for h_3 .

This is a good point to stress again the role that the LHC is having in constraining models with new scalar physics.

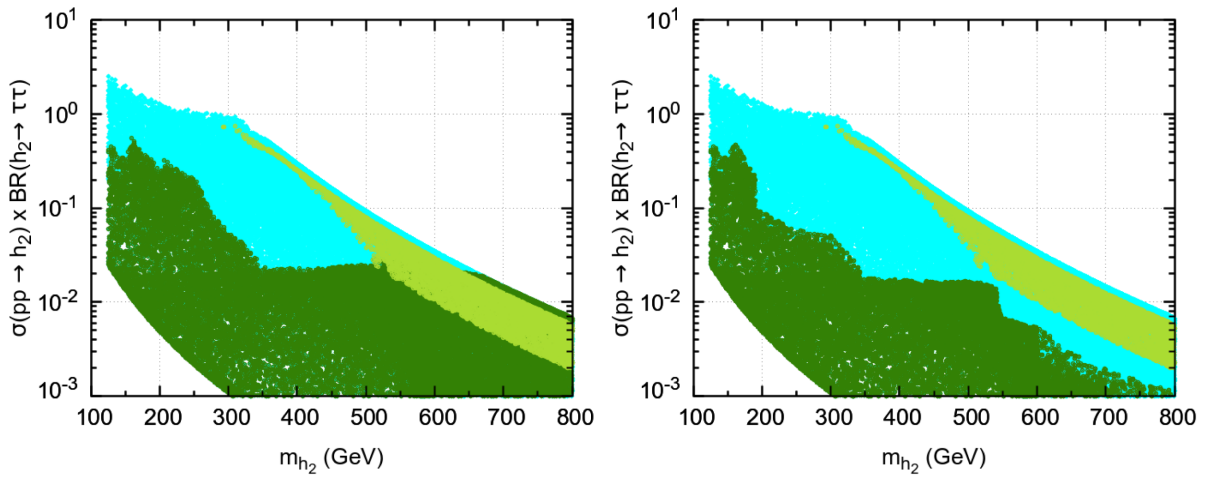


FIG. 14. Left panel: $\sigma(pp \rightarrow h_2) \times \text{BR}(h_2 \rightarrow \tau\tau)$ as function of the m_{h_2} . Parameters are as in Eq. (73), except that $\gamma_2 \in [-\pi/2, \pi/2]$. Points in cyan are points that pass all constraints before HiggsBounds and in dark green after HiggsBounds-5.7.1. In light green are the points in the interval $\gamma_2 \in [\pi/6, \pi/3]$. Right panel: the same but for HiggsBounds-5.9.1.

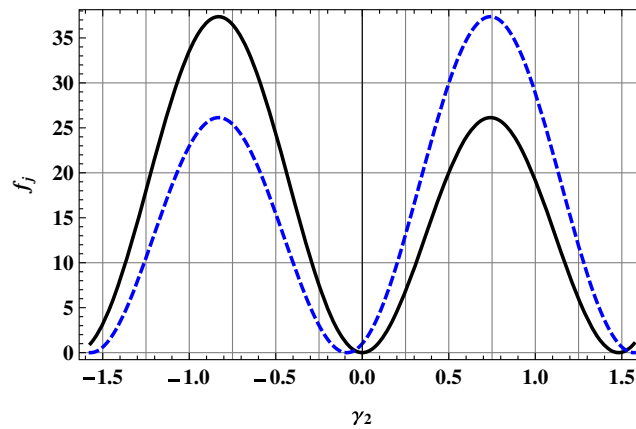


FIG. 15. Graphic of the functions f_j defined in Eq. (B1) for varying $\gamma_2 = -\alpha_3$, with $\tan\beta_1 = 10$ and $\tan\beta_2 = 2$. Function f_2 (f_3) in black/solid (blue/dashed) line.

One sees the strong impact that the updated LHC results have in constraining the Z_3 3HDM. This highlights the importance that the upcoming LHC run will have in constraining the parameter space of extended scalar sectors.

To better understand the behavior of $\sigma(pp \rightarrow h_i) \times \text{BR}(h_i \rightarrow \tau\tau)$ ($i = 2, 3$), we can make the simplified assumption¹¹ that this product is proportional to

$$\sigma(pp \rightarrow h_i) \times \text{BR}(h_i \rightarrow \tau\tau) \propto g_{h_i\tau\tau}^2 g_{h_i tt}^2 \equiv f_i, \quad (\text{B1})$$

where we are assuming that the production occurs mainly via gluon fusion with the top quark in the loop. Now, using the assumptions of Eq. (73) in Eq. (25), we have

$$\begin{aligned} g_{h_2\tau\tau} &= -\frac{c_{\alpha_3} t_{\beta_1}}{c_{\alpha_2}} - s_{\alpha_3} t_{\beta_2} = -\frac{t_{\beta_1}}{c_{\beta_2}} c_{\gamma_2} + t_{\beta_2} s_{\gamma_2}, & g_{h_2 tt} &= \frac{c_{\alpha_2} s_{\alpha_3}}{s_{\beta_2}} = -\frac{1}{t_{\beta_2}} s_{\gamma_2}, \\ g_{h_3\tau\tau} &= -c_{\alpha_3} t_{\beta_2} + \frac{s_{\alpha_3} t_{\beta_1}}{c_{\alpha_2}} = -t_{\beta_2} c_{\gamma_2} - \frac{t_{\beta_1}}{c_{\beta_2}} s_{\gamma_2}, & g_{h_3 tt} &= \frac{c_{\alpha_2} c_{\alpha_3}}{s_{\beta_2}} = \frac{1}{t_{\beta_2}} c_{\gamma_2}, \end{aligned} \quad (\text{B2})$$

where, for Fig. 14, β_1, β_2 are fixed and $\gamma_2 \in [-\pi/2, \pi/2]$. Fig. 15 shows the functions in Eq. (B1)— f_2 for h_2 and f_3 for h_3 —for $\tan\beta_1 = 10$ and $\tan\beta_2 = 2$ as in Eq. (72), but keeping γ_2 free.

We see that these functions are largest precisely in the approximate interval $\pm\gamma_2 \in [\pi/6, \pi/3]$. This explains why these points are the first to be excluded by the bounds on $\sigma(pp \rightarrow h_2) \times \text{BR}(h_2 \rightarrow \tau\tau)$, and why, going outside such bounds, some points can be preserved.¹²

¹¹We are neglecting the dependence of the cross section on the mass.

¹²Of course, we have ignored in this simple reasoning the dependence on m_{h_i} , which has been taken into account appropriately in our scans and HB5 constraints.

[1] G. Aad *et al.* (ATLAS Collaboration), Observation of a new particle in the search for the Standard Model Higgs boson with the ATLAS detector at the LHC, *Phys. Lett. B* **716**, 1 (2012).

[2] S. Chatrchyan *et al.* (CMS Collaboration), Observation of a new boson at a mass of 125 GeV with the CMS experiment at the LHC, *Phys. Lett. B* **716**, 30 (2012).

[3] J. F. Gunion, H. E. Haber, G. L. Kane, and S. Dawson, *The Higgs Hunter's Guide*, Frontiers in Physics (Westview Press, Boulder, Colorado, 2000).

[4] G. C. Branco, P. M. Ferreira, L. Lavoura, M. N. Rebelo, M. Sher, and J. P. Silva, Theory and phenomenology of two-Higgs-doublet models, *Phys. Rep.* **516**, 1 (2012).

- [5] I. P. Ivanov, Building and testing models with extended Higgs sectors, *Prog. Part. Nucl. Phys.* **95**, 160 (2017).
- [6] A. D. Sakharov, Violation of CP invariance, C asymmetry, and baryon asymmetry of the universe, *Pis'ma Zh. Eksp. Teor. Fiz.* **5**, 32 (1967).
- [7] S. L. Glashow and S. Weinberg, Natural conservation laws for neutral currents, *Phys. Rev. D* **15**, 1958 (1977).
- [8] E. A. Paschos, Diagonal neutral currents, *Phys. Rev. D* **15**, 1966 (1977).
- [9] P. M. Ferreira, L. Lavoura, and J. P. Silva, Renormalization-group constraints on Yukawa alignment in multi-Higgs-doublet models, *Phys. Lett. B* **688**, 341 (2010).
- [10] K. Yagyu, Higgs boson couplings in multi-doublet models with natural flavour conservation, *Phys. Lett. B* **763**, 102 (2016).
- [11] A. G. Akeroyd, S. Moretti, T. Shindou, and M. Song, CP asymmetries of $\bar{B} \rightarrow X_s/X_d \gamma$ in models with three Higgs doublets, *Phys. Rev. D* **103**, 015035 (2021).
- [12] H. E. Logan, S. Moretti, D. Rojas-Ciofalo, and M. Song, CP violation from charged Higgs bosons in the three Higgs doublet model, *J. High Energy Phys.* **07** (2021) 158.
- [13] D. Das and I. Saha, Alignment limit in three Higgs-doublet models, *Phys. Rev. D* **100**, 035021 (2019).
- [14] R. Boto, Symmetry-constrained multi-Higgs doublet models, Master's thesis, IST, University of Lisbon, 2021.
- [15] M. Chakraborti, D. Das, M. Levy, S. Mukherjee, and I. Saha, Prospects of light charged scalars in a three Higgs doublet model with Z_3 symmetry, [arXiv:2104.08146](https://arxiv.org/abs/2104.08146).
- [16] M. P. Bento, H. E. Haber, J. C. Romão, and J. P. Silva, Multi-Higgs doublet models: Physical parametrization, sum rules and unitarity bounds, *J. High Energy Phys.* **11** (2017) 095.
- [17] M. Misiak and M. Steinhauser, Weak radiative decays of the B meson and bounds on M_{H^\pm} in the two-Higgs-doublet model, *Eur. Phys. J. C* **77**, 201 (2017).
- [18] P. Bechtel, D. Dercks, S. Heinemeyer, T. Klingl, T. Stefaniak, G. Weiglein, and J. Wittbrodt, HiggsBounds-5: Testing Higgs sectors in the LHC 13 TeV era, *Eur. Phys. J. C* **80**, 1211 (2020).
- [19] G. Aad *et al.* (ATLAS Collaboration), Search for Heavy Higgs Bosons Decaying into Two Tau Leptons with the ATLAS Detector Using pp Collisions at $\sqrt{s} = 13$ TeV, *Phys. Rev. Lett.* **125**, 051801 (2020).
- [20] D. Fontes, M. Löschner, J. C. Romão, and J. P. Silva, Leaks of CP violation in the real two-Higgs-doublet model, *Eur. Phys. J. C* **81**, 541 (2021).
- [21] H. Georgi and D. V. Nanopoulos, Suppression of flavor changing effects from neutral spinless meson exchange in gauge theories, *Phys. Lett.* **82B**, 95 (1979).
- [22] J. F. Donoghue and L. F. Li, Properties of charged Higgs bosons, *Phys. Rev. D* **19**, 945 (1979).
- [23] F. J. Botella and J. P. Silva, Jarlskog-like invariants for theories with scalars and fermions, *Phys. Rev. D* **51**, 3870 (1995).
- [24] A. Aranda, D. Hernández-Otero, J. Hernández-Sánchez, V. Keus, S. Moretti, D. Rojas-Ciofalo, and T. Shindou, Z_3 symmetric inert $(2 + 1)$ -Higgs-doublet model, *Phys. Rev. D* **103**, 015023 (2021).
- [25] K. G. Klimenko, On necessary and sufficient conditions for some Higgs potentials to be bounded from below, *Teor. Mat. Fiz.* **62**, 87 (1985) [*Theor. Math. Phys.* **62**, 58 (1985)].
- [26] D. Fontes, J. C. Romão, and J. W. Valle, Electroweak breaking and Higgs boson profile in the simplest linear seesaw model, *J. High Energy Phys.* **10** (2019) 245.
- [27] F. S. Faro and I. P. Ivanov, Boundedness from below in the $U(1) \times U(1)$ three-Higgs-doublet model, *Phys. Rev. D* **100**, 035038 (2019).
- [28] I. P. Ivanov and F. Vazão, Yet another lesson on the stability conditions in multi-Higgs potentials, *J. High Energy Phys.* **11** (2020) 104.
- [29] W. Grimus, L. Lavoura, O. M. Ogreid, and P. Osland, A precision constraint on multi-Higgs-doublet models, *J. Phys. G* **35**, 075001 (2008).
- [30] M. Baak, J. Cúth, J. Haller, A. Hoecker, R. Kogler, K. Mönig, M. Schott, and J. Stelzer (Gfitter Group), The global electroweak fit at NNLO and prospects for the LHC and ILC, *Eur. Phys. J. C* **74**, 3046 (2014).
- [31] D. Fontes, J. C. Romão, and J. P. Silva, $h \rightarrow Z\gamma$ in the complex two Higgs doublet model, *J. High Energy Phys.* **12** (2014) 043.
- [32] D. Fontes and J. C. Romão, FeynMaster: A plethora of Feynman tools, *Comput. Phys. Commun.* **256**, 107311 (2020).
- [33] D. Fontes and J. C. Romão, Renormalization of the C2HDM with FeynMaster 2, *J. High Energy Phys.* **06** (2021) 016.
- [34] P. Nogueira, Automatic feynman graph generation, *J. Comput. Phys.* **105**, 279 (1993).
- [35] N. D. Christensen and C. Duhr, FeynRules-Feynman rules made easy, *Comput. Phys. Commun.* **180**, 1614 (2009).
- [36] A. Alloul, N. D. Christensen, C. Degrande, C. Duhr, and B. Fuks, FeynRules 2.0: A complete toolbox for tree-level phenomenology, *Comput. Phys. Commun.* **185**, 2250 (2014).
- [37] R. Mertig, M. Bohm, and A. Denner, FEYN CALC: Computer algebraic calculation of Feynman amplitudes, *Comput. Phys. Commun.* **64**, 345 (1991). Available at <https://www.feyncalc.org/>.
- [38] V. Shtabovenko, R. Mertig, and F. Orellana, New developments in FeynCalc 9.0, *Comput. Phys. Commun.* **207**, 432 (2016).
- [39] G. Aad *et al.* (ATLAS Collaboration), Combined measurements of Higgs boson production and decay using up to 80 fb⁻¹ of proton-proton collision data at $\sqrt{s} = 13$ TeV collected with the ATLAS experiment, *Phys. Rev. D* **101**, 012002 (2020).
- [40] M. Spira, HIGLU: A program for the calculation of the total Higgs production cross-section at hadron colliders via gluon fusion including QCD corrections, [arXiv:hep-ph/9510347](https://arxiv.org/abs/hep-ph/9510347).
- [41] D. de Florian *et al.* (LHC Higgs Cross Section Working Group), Handbook of LHC Higgs cross sections: 4. Deciphering the nature of the Higgs sector, [arXiv:1610.07922](https://arxiv.org/abs/1610.07922).
- [42] J. C. Romão and S. Andringa, Vector boson decays of the higgs boson, *Eur. Phys. J. C* **7**, 631 (1999).
- [43] A. Djouadi, The Anatomy of electro-weak symmetry breaking. I: The Higgs boson in the standard model, *Phys. Rep.* **457**, 1 (2008).
- [44] A. Barroso, P. M. Ferreira, R. Santos, and J. P. Silva, Probing the scalar-pseudoscalar mixing in the 125 GeV Higgs particle with current data, *Phys. Rev. D* **86**, 015022 (2012).
- [45] F. Borzumati and C. Greub, 2HDMs predictions for anti-B \rightarrow X(s) gamma in NLO QCD, *Phys. Rev. D* **58**, 074004 (1998).

- [46] F. Borzumati and C. Greub, Two Higgs doublet model predictions for anti- $B \rightarrow X(s) \gamma$ in NLO QCD, *Phys. Rev. D* **59**, 057501(A) (1999).
- [47] M. Misiak, Radiative decays of the B meson: A progress report, *Acta Phys. Pol. B* **49**, 1291 (2018).
- [48] F. U. Bernlochner, H. Lacker, Z. Ligeti, I. W. Stewart, F. J. Tackmann, and K. Tackmann (SIMBA Collaboration), Precision Global Determination of the $B \rightarrow X_s \gamma$ Decay Rate, *Phys. Rev. Lett.* **127**, 102001 (2021).
- [49] Y. S. Amhis *et al.* (HFLAV Collaboration), Averages of b -hadron, c -hadron, and τ -lepton properties as of 2018, *Eur. Phys. J. C* **81**, 226 (2021).
- [50] M. Misiak, A. Rehman, and M. Steinhauser, Towards $\bar{B} \rightarrow X_s \gamma$ at the NNLO in QCD without interpolation in m_c , *J. High Energy Phys.* **06** (2020) 175.
- [51] J. L. Hewett, Top ten models constrained by $b \rightarrow s \gamma$, in *Proceedings of the 21st Annual SLAC Summer Institute on Particle Physics: Spin Structure in High-energy Processes (SSI 93)* (SLAC, Stanford, California, 1994), p. 5, [arXiv:hep-ph/9406302](https://arxiv.org/abs/hep-ph/9406302).
- [52] A. G. Akeroyd, S. Moretti, K. Yagyu, and E. Yildirim, Light charged Higgs boson scenario in 3-Higgs doublet models, *Int. J. Mod. Phys. A* **32**, 1750145 (2017).
- [53] P. A. Zyla *et al.* (Particle Data Group), Review of particle physics, *Prog. Theor. Exp. Phys.* **2020**, 083C01 (2020).
- [54] CMS Collaboration, Search for additional neutral Higgs bosons decaying to a pair of tau leptons in pp collisions at $\sqrt{s} = 7$ and 8 TeV, CMS-PAS-HIG-14-029.
- [55] CMS Collaboration, Search for additional neutral MSSM Higgs bosons in the di-tau final state in pp collisions at $\sqrt{s} = 13$ TeV, CMS-PAS-HIG-17-020.
- [56] R. R. Florentino, J. C. Romão, and J. P. Silva, Off diagonal charged scalar couplings with the Z boson: the Zee model as an example, [arXiv:2106.08332](https://arxiv.org/abs/2106.08332).
- [57] H. Bahl, T. Stefaniak, and J. Wittbrodt, The forgotten channels: Charged Higgs boson decays to a W^\pm and a non-SM-like Higgs boson, *J. High Energy Phys.* **06** (2021) 183.